Cascaded Stalling of Induction Motors in Fault-Induced Delayed Voltage Recovery (FIDVR)

by

Heng Chen

A thesis submitted in fulfillment of the

requirements for the degree of

Master of Science

(Electrical Engineering)

at the

UNIVERSITY OF WISCONSIN-MADISON

2011

Abstract

In recent years, the phenomenon of Fault-Induced Delayed Voltage Recovery (FIDVR) has increasingly been observed. Air conditioner (A/C) motor stalling is considered as one of the main reasons for the occurrence of delayed voltage recovery events [3]. This thesis studies the possibility that the stalling of a small percentage of induction motors could precipitate FIDVR events. A 12.5kV distribution network model with A/C motor load is used to construct certain bifurcation diagrams. Continuation methods based on the predictor-corrector technique are used to arrive at system steady-state solutions tracing the curves of motor behavior while the system bus voltage is varied.

The stable and unstable operating points of induction machines are obtained and analyzed. Results show that a small percentage of induction motors stalling could exacerbate the stalling of additional motors. There could be either no stable solutions for the system with a partial number of A/C motors stalled or stable solutions with a certain number of A/C motors stalled, depending on the percentage of integrated motor loads. We conclude that a small percentage of stalled induction motors in practice could precipitate the stalling of additional motors, or even all motors in a distribution network. Thus, a mitigation strategy of replacing a number of "prone to stall" motors to "robust" ones may not effective. This information is crucial in developing mitigation plans to avoid a FIDVR event.

Acknowledgements

I would like to give my sincerest gratitude to my advisor, Professor Bernard C. Lesieutre, for giving me the opportunity to pursue this research. His insightful ideas about Power Systems and Energy Analysis and Policy, and cheerful attitude have been an enlightening source of my growth as a master student. I am deeply indebted to him for all his excellent guidance, support and help. His influence on my study and research reaches far beyond this thesis.

I would like to thank many of my fellow graduate students at UW – Madison, and the members of the Wisconsin Power Engineering Research Center (WisPERC) in particular, Honghao Zheng, Dan Molzahn, Chaitanya Baone, Alex Borden, Vikas Dawar, Rafeal Viloria, and Kanishka Kumar, for their friendship and making this experience memorable and enjoyable.

My deepest gratitude to my parents, for their constantly love, encourage, and support during my life. This work and my education would not have been made possible without them.

I would like to acknowledge Bonneville Power Administration (BPA) and National Science Foundation (NSF) for their generous support for this work.

Table of Contents

List of Tables

List of Figures

1. Introduction

Increases in load demand and power transfer between utilities raise concern for voltage stability in electric power systems. Beyond the natural complexity and dynamics of the system, the integration of renewable generation, which may behave intermittently, and the political and environmental resistance to the upgrade or construction of new transmission lines is forcing the power grid to rely on existing generation and transmission facilities. This situation would make the system operate closer to the operating limit, which leads to increasing concern of voltage stability [1].

Load characteristics play an important role in the dynamic behavior of the power systems. Throughout the years, numerous studies have shown that proper modeling of loads used in both real time operation and post event analysis. However, loads may not be modeled accurately enough to capture the inherent nature or predict how the load would look like at any point during a particular event. In recent years, there has been an increasing concern about the load model of induction motors, especially air conditioner (A/C) motors. Induction motors constitute a major portion of loads in power systems. It appears necessary to account accurately for induction motors in dynamic and transient stability studies of power systems. It has been found that in the event of a system fault, the stalling behavior of A/C motors may lead to delayed voltage recovery [2], which may potentially lead to cascaded stalling of other induction motors within the same distribution feeder or the nearby ones, and eventually it might lead to a system voltage collapse [3].

Fault-Induced Delayed Voltage Recovery is the phenomenon whereby system voltage remains at significantly reduced levels for several seconds after a transmission, subtransmission, or distribution fault has been cleared. The North American Electric Reliability Corporation (NERC) Transmission Issues Subcommittee provides the following definition for FIDVR in their recently published white paper [3]:

Fault-Induced Delayed Voltage Recovery (FIDVR) — a voltage condition initiated by a fault and characterized by:

- *Stalling of induction motors*
- *Initial voltage recovery after the clearing of a fault to less than 90% of pre-contingency voltage*
- *Slow voltage recovery of more than 2 seconds to expected post-contingency steady-state voltage levels*

A typical FIDVR is shown in Figure 1. System voltage can be significantly depressed for seconds after the fault is cleared, mainly because induction motors require typically 5-6 times their steady-state current in the locked-rotor condition. Eventually, the stalled motors will trip by thermal protection with an inverse time-overcurrent characteristic. This can take from 3 to 20 seconds.

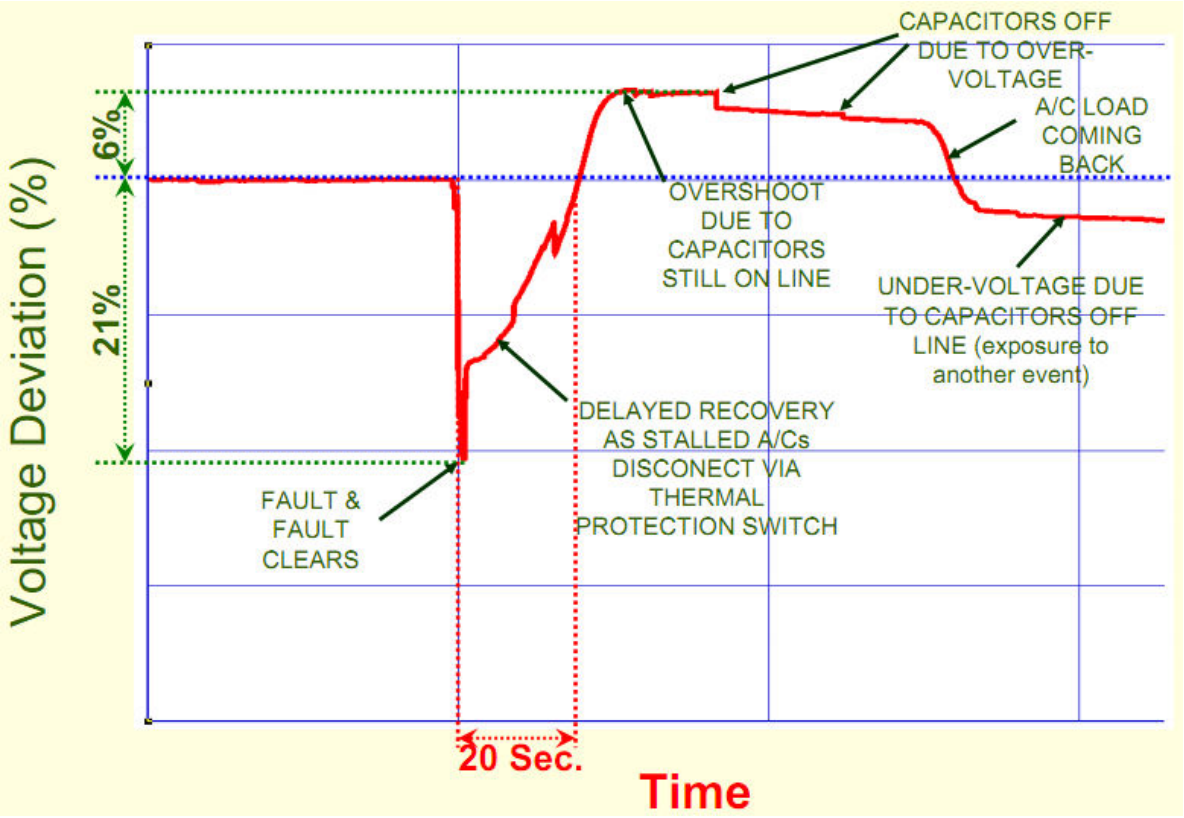

Figure 1. Typical FIDVR Following a 230-kV Transmission Fault [3]

FIDVR events seem to occur more frequently than in past years because the density of induction motors is increasing with continuing market penetration of low-inertia air conditioning loads without compressor undervoltage protection. Back in 1988, John W. Shaffer of Florida Power and Light Company (FPL) reported an event in [4]. A bolted 3-phase fault at the Flagami 230-kV switching station initiated the event. Although the fault was cleared in 3.5 cycles, approximately 825 MW of load was disconnected in the Miami area, almost all due to customer equipment protection. Six feeder breakers were tripped by time over current relays just after the fault. Area transmission voltage was depressed for ten seconds after fault isolation.

Multiple FIDVR events occurred in Southern California Edison's desert regions during the peak air-conditioning period, including a major incident in June, 1990, which affected a 1000 square mile area of Riverside County [2]. The paper also points to FIDVR incidents in the other utilities like Sacramento Municipal Utility District, Kansas Gas & Electric area, etc. The combination of high percentages of motor loads, long heavily loaded lines, and slow clearing faults appear to be major causes of these voltage recovery problems.

Utilities are beginning to adequately model and study FIDVR. Southern California Edison has determined that its A/C load penetration is 25% of coastal load and up to 60% of inland load on peak [3]. Southern Company (SOCO) is one leader in the Eastern Interconnection in going beyond modeling and studying FIDVR to also educate others in the industry to the phenomenon and the requirements for its study and mitigation. SOCO has widely published the lessons learned from its Union City event in 1999. However, many North American electric utilities lack the models and the knowledge to adequately study and plan for FIDVR. Simply determining the motor load as percent of total load can be challenging.

Induction motor penetration is one of the most critical parameters that determine a transmission system's susceptibility to FIDVR events. Highly concentrated induction motor loads with constant torque could stall in response to low voltages associated with system faults and draw excessive reactive power from the grid. "Prone to stall" motors, usually small, single-phase induction motors found in A/C equipment having low inertia, can stall for nearly all faults greater than five cycles as a result of fault voltages less than 60% nominal value [2]. But not all motors are vulnerable to stalling. Large industrial motors often have

contactors that will trip them offline during voltage drops, thus limiting the negative impact of these motors. For instance, large HVAC units may also have motor protection that will cut the unit out before stalling occurs. Smaller HVAC units, however, may not have protection that will trip the unit off before stalling occurs. The mechanical torque of the compressor for these units tends to remain relatively constant which makes the motors more prone to stalling. Under a severe situation, larger induction motors can also tend to stalling, though they should be slightly slower to stall and should do so at lower system voltage due to their larger inertia. Stalled induction motors present a high reactive loading to the transmission system further aggravating the initial fault voltage depression [3].

In [3], NERC Transmission Issues Subcommittee suggests both grid level and unit level solutions to FIDVR event. Grid level solutions include quicker clearing of faults, addition of reactive sources, limiting impacted load, etc. These solutions could contain the events by limiting their area of influence and consequences, but they cannot ensure prevention of FIDVR events. Unit level solutions focus on promotion of grid-friendly A/C units with equipment control devices to remove induction motor loads from the grid prior to stalling for undervoltage conditions. This is a component of the long term solution. However, A/C standards necessary to achieve this will not be enacted overnight and to retrofit of existing A/C units could be even more difficult to accomplish. It is still uncertain that whether replacing a number of “prone to stall” motors to “robust” ones would be able to mitigate FIDVR events or not. If the stalling of a small percentage of induction motors could exacerbate the stalling of additional motors, then this mitigation strategy may be ineffective.

Therefore, in this thesis, studies are conducted on a 12.5kV distribution network in order to determine the possibility of feasible solutions of the system with a few induction motors stalled. Two scenarios with different percentage of induction motor load integration are considered. In scenario 1, all the load demand is replaced by steady-state induction motor load; Scenario 2 includes fifty percent motor load and fifty percent constant impedance load. Two approaches are performed to construct appropriate bifurcation diagrams of steady-state solution curves for all induction motor loads. Firstly, the algorithm presented in [1] is implemented to find all the solutions to load flow equations. This algorithm is based on the analysis of the topological structures of the solution set defined by the parameterized load flow equations. The author claims load flow solutions are connected by one-dimension manifolds (curves) to form a connected graph, and all the load flow solutions can be found by tracing these curves. For our distribution system with aggregate induction motor models, results indicate that the only stable solutions at nominal voltage are all the induction motors operating in the normal condition.

A second approach, continuation power flow based on predictor-corrector technique, is conducted to arrive at system steady-state solutions tracing the curves of motor behavior while the system bus voltage is varied. From the reasonable solution of the normal operating point, the continuation method traces the system bus voltage magnitude downwards. The induction motors that stall during this process are switched to stall condition model accordingly, giving the motor slip equals to one afterwards. The stable and unstable operating range of induction machines is obtained and analyzed. The results indicate the stalling of a number of A/C motors could lead to the stalling of additional motors, and the only stable solutions at nominal voltage are with all induction motors stalled.

Based on our work, we conclude that a small percentage of stalled induction motors in practice could precipitate the stalling of additional motors, or even all motors in a distribution network. Thus, the mitigation strategy that replacing a number of "prone to stall" motors to "robust" ones may not effective for FIDVR events.

This thesis is organized as follows. Chapter 2 presents the distribution system and load model used in the simulation. An analytical approach to aggregate a large number of A/C motors in the system is conducted. Chapter 3 presents the two approaches implemented to arrive at the system steady-state solutions. The numerical method in [1] and the continuation tracing over system bus voltage are explained in detail. The results of A/C motors behavior and system stable solutions are obtained and analyzed. Chapter 4 concludes the thesis and makes recommendations for future work.

2. System and Load Model

For the work in this thesis, a 12.5kV distribution system is used to analyze induction motors' behavior in FIDVR event. For constructing the bifurcation diagrams, a steady state induction machine model is used in the simulation. When one of the motors stalls, we "lock" the rotor speed at zero. Details are presented in section 2.2.

2.1 Distribution Network Model

The topology of the 12.5kV distribution network is shown in Figure 2.

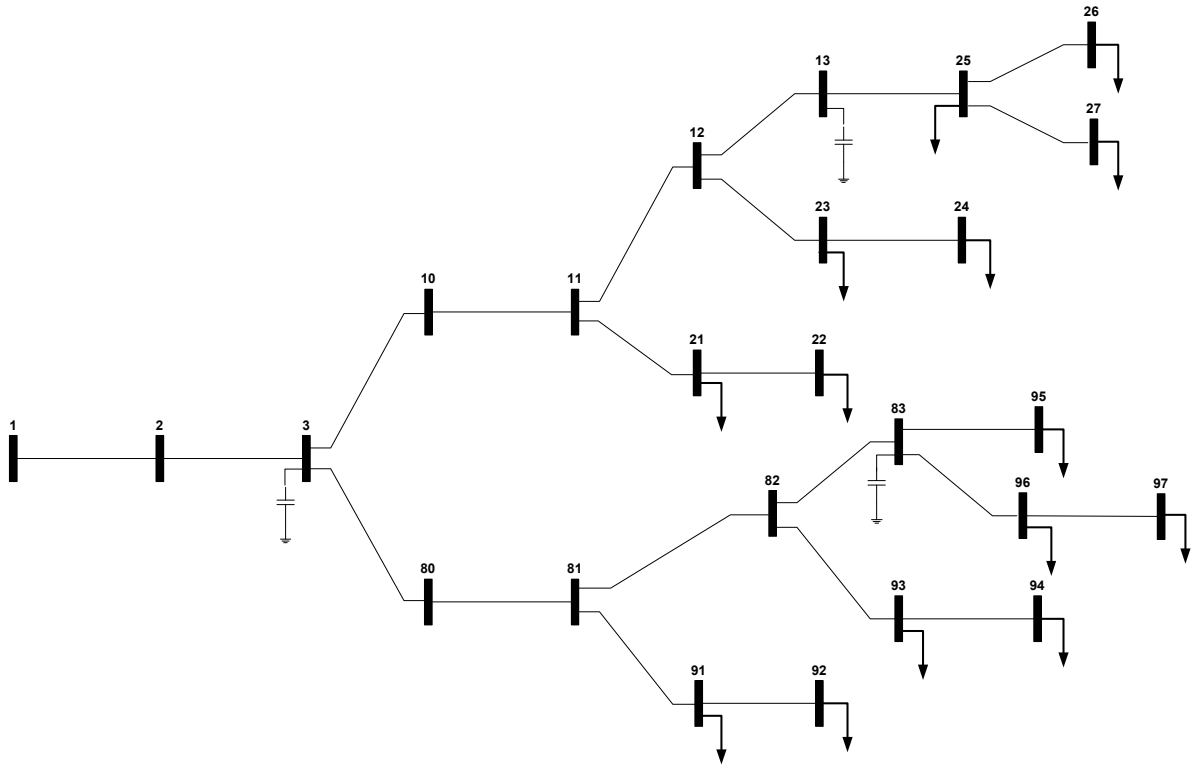

Figure 2. A Reasonable 12.5kV Distribution Network

This 25 buses system has one system slack bus at 115kV voltage level. After a certain distance of transmission line following a voltage step down transformer, we have the

leading bus of the distribution network at 12.5kV voltage level. Two feeders with similar topology are connected to this bus, and each of them has seven loads and one capacitor bank reactive power compensation as shown in figure 2.

2.2 Individual A/C Motor Model

A steady-state individual induction motor model is shown in Figure 3. The model was then applied as the load model in the distribution system.

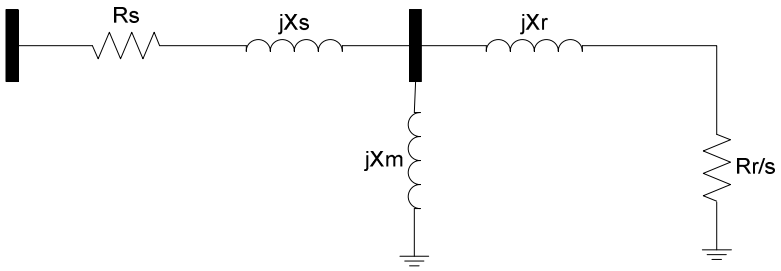

Figure 3. Individual Induction Motor Model

The motor base of the individual A/C unit was 5.7 kVA, 240V base. All impedance values are in per unit on motor base as typical values found in [6].

The load impedance in the distribution system is the combined impedance of the induction motors and other load. In our model in scenario 1, the non-motor loads are neglected. For an induction motor, the torque applied to the rotor is equal to the power delivered to the speed dependent resistor (Rr/s) shown in Figure 3. Typical A/C mechanical load is taken to use constant. This allows us to replace the speed dependent resistor with a constant power load in the model. This is shown is Figure 4. The advantage of the model in Figure 4 is that it can be analyzed using traditional power flow tools. To implement these

loads to a power flow, we have to add additional 2 buses to the system, making the distribution system 53 buses in total. The ordering of new bus numbers are listed in Table 1.

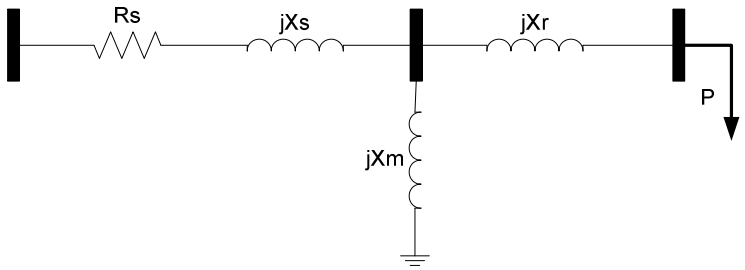

Figure 4. Modified Individual Induction Motor Model

Table 1. Numbering of New Buses in the Distribution System

Linked to bus #	21	22	23	24	25	26	27
Additional bus #	30,31	32,33	34,35	36,37	38,39	40,41	42,43
Linked to bus #	91	92	93	94	95	96	97
Additional bus #	100,101	102,103	104,105	106,107	108,109	110,111	112,113

When the system voltage drops, light inertia induction motors tend to lose their speed rapidly. This is especially true since the mechanical back pressure of the compressor quickly slows the low-inertia motor past the point where it cannot reaccelerate to full speed even if full voltage is restored [2]. When a certain motor stalls, its slip reaches 1. In that case, the motor load can not be treated as constant active power anymore. Thus, we switch the motor model again simply changing the constant power representation to a constant rotor resistance linked to the end bus. This individual induction motor model in stalling condition is shown in Figure 5.

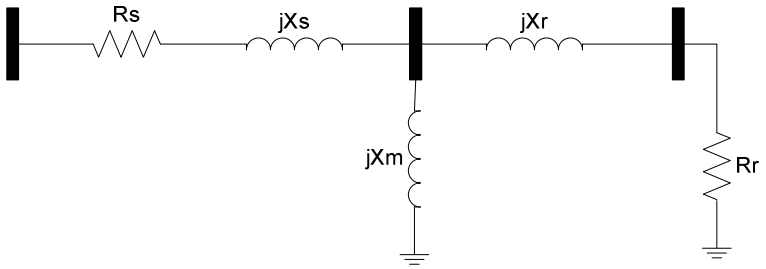

Figure 5. Individual Induction Motor Model in Stalling Condition

The model switch is done while running the continuation power flow. Beyond this point, the stalled motor will draw a lot of reactive power from the grid, which will in turn affect the system voltage and the behavior of A/C motors nearby.

2.3 Aggregate Equivalent A/C Load Model On a System-Wide Basis

It is a prohibitive task, for a steady state simulation, to include several types of induction motors and all of them in modeling of critical power system loads. To apply the individual induction motor model on a system-wide basis, it is appropriate to model a diverse group of induction motors connecting to one load bus by one aggregate equivalent motor.

Several techniques for representing induction motor loads and aggregation of induction motors have been proposed in the literature. A brief description of widely known techniques is given in the summary report of the project [7]. Also note that nearly all the available motor aggregation techniques use some form of KVA weighted averaging. The outcomes of all methods are approximate in nature, and the degrees of accuracy of all methods seem to be similar [8]. In addition, none of the methods were clearly superior to a simple weighted average method. Therefore, we choose to use the simple KVA weighted average method for the load model synthesis, which is straightforward and intuitively clear.

For this method, each parameter of the aggregate motor is calculated as the weighted average of the respective parameter of individual motors in the group, as shown in the relevant equation below.

$$X_{agg} = \sum_{j=1}^{n} \alpha_j X_j$$

Where α_j is the weighting coefficient, X_j is substituted by each parameter of the induction motor model, and X_{agg} is the associated parameter value for the aggregate motor. The weighting coefficient is defined as the ratio of the KVA rating of the individual motor with respect to the KVA rating of the aggregate motor.

$$\alpha_j = {KVA_j}/{KVA_{agg}}$$

Note that in this work, we use the same individual induction motor model for all the motor loads, so the aggregate motor parameter values are proportional to the individual ones, which are just the original value multiplied by a scalar. In addition, there is also a voltage base difference between the aggregate model and the distribution system. Thus, a voltage base change is needed, which is done as shown in the equation below:

$$X_{agg\_new} = {V_{system}^2}/{V_{motor}^2} * X_{agg\_old}$$

Where V_{system} is the base voltage of the distribution system and V_{motor} is the base voltage of the aggregate motor model.

Finally we note that the induction motor model used here corresponds to a three-phase motor. Mandy A/C compressors use single-phase motors, the characteristics of which

are believed to make them comparably more prone to stall. Thus the results in this thesis may be reviewed as “best-case” results.

3. Simulation Approach and Results

In this chapter we detail the study process and present results. Two loading scenarios are considered: 100% motor load, and 50% motor/50% impedance load. The distribution system model presented in the previous chapter is used.

The steps in the analysis are:

1. Run power flow on base case system to establish the operating point.
2. Augment the power flow model to include induction motor loads, as described in Chapter 2.
3. Initialize the augmented model to match the operating point.
4. Construct bifurcation diagrams of feasible solutions as a function of system voltage.
5. Analyze the curves to determine the number of stable feasible solutions at nominal voltage.

The algorithm in [1] with load active power and reactive power as tracing parameters is used to find all load flow solutions of the given network. At 1.3 per unit voltage, 14 solutions are found for the 100% motor load scenario; at 1.0 per unit voltage, 26 solutions are found for the 50% motor/50% impedance load scenario. Then starting from these reasonable solution, a continuation method is applied with the slack bus voltage as the tracing parameter to find induction motors' behavior with decreasing voltage. During this process, we need to switch the model for stalled induction motors to stall condition and keep decreasing slack bus voltage to eventually get all motors' stalling behavior. Details of the simulation and results are presented in the following sections.

3.1 Steady-state Power Flow Analysis

A steady state power flow is conducted to find a normal operating point of the given distribution system using MATPOWER. MATPOWER is a package of MATLAB M-files for solving power flow and optimal power flow problems. In MATPOWER, by convention, a single generator bus is typically chosen as a reference bus to serve the roles of both a voltage angle reference and a real power slack, which is the slack bus in our case. The voltage angle at the reference bus has a known value, but the real power generation at the slack bus is taken as unknown to avoid over specifying the problem. Since the loads are also given, all the remaining buses are PQ buses, with real and reactive injections fully specified. The data format for the input can be found in [9].

MATPOWER's default AC power flow solver is based on a standard Newton's method using a polar form and a full Jacobian updated at each iteration. Each Newton step involves computing the new mismatch, forming the Jacobian based on the sensitivities of these mismatches to changes in variables and solving for an updated value of voltage magnitudes and angles by factorizing this Jacobian.

This technique is used to find the first normal solution to the distribution system. Details are presented in Section 3.3 and Section 3.4.

3.2 Finding All Load Flow Solutions

Mathematically, the power flow problem consists of the solution of a large sparse set of nonlinear algebraic equation. Existence of solutions, convergence of a solver, multiple solutions, bifurcations and approximations are some of the issues that are generally

associated with nonlinear equations. These issues are also of concern for the power flow problem. A particular difficulty being encountered in such research is that the Jacobian of a Newton-Raphson power flow becomes singular at the critical point. As a consequence, attempts to find power flow solutions near the critical point are prone to divergence and error. Singularity in the Jacobian can be avoided by slightly reformulating the power flow equations and applying a locally parameterized continuation technique. The reformulated set of equations remains well-conditioned so that divergence and error are not encountered. Continuation methods are slow but extremely robust and powerful [10]. They are typically well suited to study severe voltage problems.

Continuation methods have been used for many years in power systems in a variety of applications [11–14]. The general principle behind the continuation power flow is not complicated. The nonlinear equations can be reformulated by introducing a load parameter into the original system. The procedure follows a path starting at a known solution for a known value of the chosen parameter up to either an unspecified value of the parameter or to a specific value of the parameter. In either case, it employs a predictor-corrector scheme to find the next solution along the path of a set of power flow equations. As shown in Figure 6, based on present and past information, it uses a tangent predictor to predict a solution at a point in the path for a larger value of the load parameter. This estimate is then corrected using iteration until and actual solution along the path is obtained. The corrector step could be the same Newton-Raphson technique employed by a conventional power flow. Detail explanations of the predictor-corrector scheme can be found in [15].

For a range of values of load parameter, it is possible to identify each solution on the path in a mathematical way. Problems arise when a solution does not exist for some maximum possible parameter value. At this point, one of the state variables can be used effectively as the parameter to be varied, the choice of which is determined locally at each continuation step. The continuation method can be requested to calculate the point on the curve at specified parameter values. Therefore, if we apply the continuation method to the power flow equations with the same point as the terminating condition, and with the request to calculate the special points on the curve where parameter equals to zero, we trace a smooth loop of solutions exactly once and find all the load flow solutions connected by it.

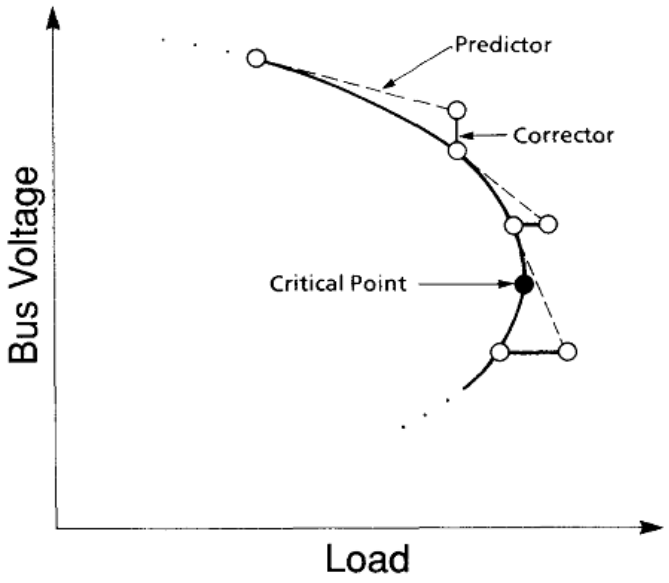

Figure 6. An Illustration of the Predictor-Corrector Scheme [15]

The author in [1] developed a novel, numerically efficient algorithm to locate all the load flow solutions using the continuation method. However, we argue that the method has not been proven to find all solutions, and a counter example is given in the Appendix showing part of the author's proof is wrong. Nevertheless, the method may find all the

solutions, even if not proven to do so. The algorithm is based on the analysis of the topological structure of the parameterized load flow equations, which is also the mathematical foundation of the algorithm. Special symmetric structures are identified on the solution sets of both the original load flow equations and the parameterized load flow equations to avoid unnecessary repetition. It turns out that the solution set of the parameterized load flow equations specified by allowing only one of the parameter to vary is generically a one-dimensional manifold, and his manifold connects every solution point of the original load flow equation to at least another solution point. A set of manifolds corresponding to different parameters forms a connected graph with the solution points being the nodes and the manifolds being the branches. These manifolds connect the solutions to each other, and thus can be traced by the continuation method. Each trace is guaranteed to find at least another solution. This process stops when all the solutions are found. However, the total number of the solutions is not known until after all the solutions are found, which means we can not determine all the solutions are found by counting the number of the solutions found so far. Therefore, we need to ensure that the set of branches of the manifold is traced. It is desirable that this set of manifold branches is a minimal set to avoid wasting computation time.

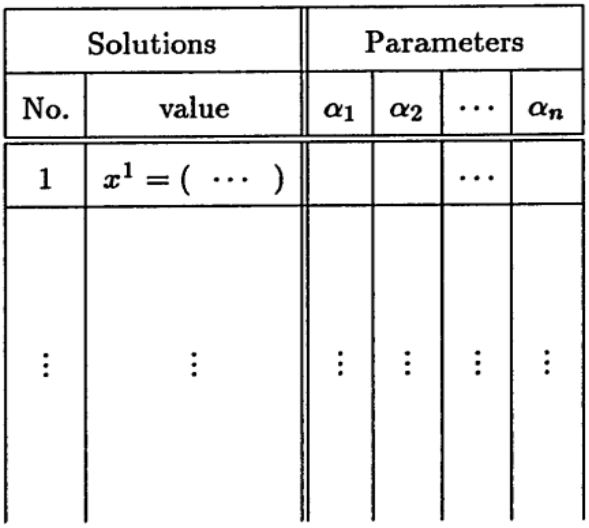

Figure 7. Book Keeping Table For the Continuation Trace – Start [1]

The algorithm presented by the author systematically organizes the traces [1]. One can first set up a table with n columns and s rows, as shown in Figure 7. Each column corresponds to a parameter, and each row corresponds to a solution. There is a freedom of choosing either of these parameter set. Since the total number of the solutions is not known yet, the table is an open ended one. Staring from the first row of known solution, each blank space (i, j) in the table represents a starting combination of the continuation trace. Thus, the new trace will start at the i-th solution point, trace the manifold with j-th parameter. The traced curve will end at the starting point. During this process, any point on this curve corresponding to a zero parameter value is recorded as a solution. If it is an old solution, the corresponding space in the table will be marked. If it is a new solution, it is appended to the end of the table and the corresponding space will be marked. This process ends when all the spaces are marked, as shown in Figure 8.

Solutions		Parameters			
No.	value	α_1	α_2	$\cdots$	α_n
1	$x^1 = (\ \cdots\ )$	×	×	$\cdots$	×
2	$x^2 = (\ \cdots\ )$	×	×	$\cdots$	×
$\vdots$	$\vdots$	$\vdots$	$\vdots$	$\vdots$	$\vdots$
s	$x^s = (\ \cdots\ )$	×	×	$\cdots$	×

Figure 8. Book Keeping Table For the Continuation Trace – Finish [1]

3.3 Distribution System Base Case Simulation

A steady state power flow is first conducted to find normal operating point of the base case using MATPOWER. For the given system, Newton's method converges fast, and the simulation result of the distribution system base case is shown in Table 2. (The distribution system and labeled buses are shown in Figure 2.)

Table 2. Simulation Results of the Distribution System Base Case

Bus #	Voltage Mag(pu)	Voltage Ang(deg)	Generation P (MW)	Generation Q (MVAr)	Load P (MW)	Load Q (MVAr)
1	1.020	0.000	14.84	3.78	-	-
2	0.956	-8.191	-	-	-	-
3	0.968	-15.137	-	-	-	-
10	0.967	-15.143	-	-	-	-
11	0.964	-15.556	-	-	-	-
12	0.959	-16.782	-	-	-	-
13	0.958	-17.554	-	-	-	-
21	0.957	-15.713	-	-	1.00	0.60

22	0.951	-15.926	-	-	1.00	0.25
23	0.946	-17.209	-	-	1.00	0.25
24	0.939	-17.427	-	-	1.00	0.25
25	0.937	-18.092	-	-	1.00	0.25
26	0.933	-18.147	-	-	1.00	0.60
27	0.930	-18.315	-	-	1.00	0.25
80	0.967	-15.138	-	-	-	-
81	0.963	-15.533	-	-	-	-
82	0.960	-16.120	-	-	-	-
83	0.959	-16.881	-	-	-	-
91	0.959	-15.584	-	-	1.00	0.60
92	0.955	-15.636	-	-	1.00	0.60
93	0.951	-16.224	-	-	1.00	0.60
94	0.947	-16.277	-	-	1.00	0.60
95	0.952	-17.093	-	-	1.00	0.25
96	0.955	-16.959	-	-	1.00	0.60
97	0.949	-17.173	-	-	1.00	0.25
			--------	--------	--------	--------
	Total:		14.84	3.78	14.00	5.95

3.4 Scenario 1: Distribution Network with 100% Motor Loads

In this section we analyze the scenario with 100% motor loads.

3.4.1 Distribution System Base Case Simulation with One Hundred Percent Aggregate Induction Motor Loads and Reactive Power Compensation

The first step in simulating this scenario is to create an augmented power flow case which matches the prefault system conditions. With the aggregate induction motor models embedded into the network, the voltage drops dramatically because of the large magnetizing reactance branches within the A/C motor models, which are considered to be shunt reactance to the system. They draw a huge amount of reactive power from the grid so that the system cannot support the voltage.

Thus, reactive power compensation is needed to the system to get a case to match the normal operating point. Here, fixed capacitor bank local compensation is added in parallel to the induction motor load model. The modified model with shunt capacitor bank is shown in Figure 9.

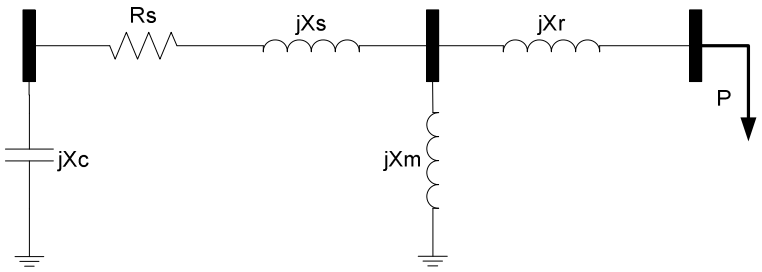

Figure 9. Modified Individual Induction Motor Model with Reactive Power Compensation

With the reactive power compensation, steady-state power flow analysis is conducted, and the results are shown in Table 3. The solution is close to the original condition, so this modified system is used for further analysis. (The numbering of new buses is shown in Table 1.)

Table 3. Simulation Results of Distribution System Base Case with Aggregate Induction Motor Loads after Reactive Power Compensation

Bus #	Voltage Mag(pu)	Voltage Ang(deg)	Generation P (MW)	Generation Q (MVAr)	Load P (MW)	Load Q (MVAr)
1	1.020	0.000	16.78	4.01	-	-
2	0.952	-9.349	-	-	-	-
3	0.968	-17.203	-	-	-	-
10	0.967	-17.210	-	-	-	-
11	0.964	-17.675	-	-	-	-
12	0.958	-19.044	-	-	-	-
13	0.957	-19.911	-	-	-	-
21	0.957	-17.887	-	-	-	-
22	0.949	-18.102	-	-	-	-
23	0.942	-19.481	-	-	-	-
24	0.935	-19.705	-	-	-	-

25	0.934	-20.580	-	-	-	-
26	0.930	-20.695	-	-	-	-
27	0.926	-20.811	-	-	-	-
80	0.967	-17.211	-	-	-	-
81	0.965	-17.671	-	-	-	-
82	0.961	-18.345	-	-	-	-
83	0.960	-19.196	-	-	-	-
91	0.961	-17.776	-	-	-	-
92	0.957	-17.882	-	-	-	-
93	0.954	-18.559	-	-	-	-
94	0.950	-18.667	-	-	-	-
95	0.953	-19.409	-	-	-	-
96	0.957	-19.302	-	-	-	-
97	0.949	-19.517	-	-	-	-
30	0.924	-16.983	-	-	-	-
31	0.924	-17.252	-	-	1.00	0.00
32	0.916	-17.204	-	-	-	-
33	0.916	-17.478	-	-	1.00	0.00
34	0.910	-18.587	-	-	-	-
35	0.910	-18.865	-	-	1.00	0.00
36	0.902	-18.817	-	-	-	-
37	0.902	-19.099	-	-	1.00	0.00
38	0.901	-19.693	-	-	-	-
39	0.901	-19.976	-	-	1.00	0.00
40	0.897	-19.810	-	-	-	-
41	0.897	-20.096	-	-	1.00	0.00
42	0.894	-19.929	-	-	-	-
43	0.894	-20.217	-	-	1.00	0.00
100	0.928	-16.869	-	-	-	-
101	0.927	-17.136	-	-	1.00	0.00
102	0.924	-16.978	-	-	-	-
103	0.924	-17.247	-	-	1.00	0.00
104	0.921	-17.657	-	-	-	-
105	0.921	-17.928	-	-	1.00	0.00
106	0.917	-17.768	-	-	-	-
107	0.917	-18.041	-	-	1.00	0.00
108	0.920	-18.508	-	-	-	-
109	0.920	-18.780	-	-	1.00	0.00
110	0.923	-18.398	-	-	-	-
111	0.923	-18.668	-	-	1.00	0.00
112	0.916	-18.619	-	-	-	-
113	0.916	-18.893	-	-	1.00	0.00
		Total:	16.78	4.01	14.00	0.00

3.4.2 Simulation and Results of Induction Motor Stalling in FIDVR

Finding all the solutions of the modified system in Section 3.4.1 is our first goal. With the technique discussed above, a continuation method with all load active power and reactive power as tracing parameters is used to find all load flow solutions of the given network. In this case, we have 53 buses with 104 nonlinear equations. 14 solutions are found after 693 tracing processes when slack bus voltage equal to 1.3 per unit. The voltage magnitudes of these 14 solutions are shown in Figure 10.

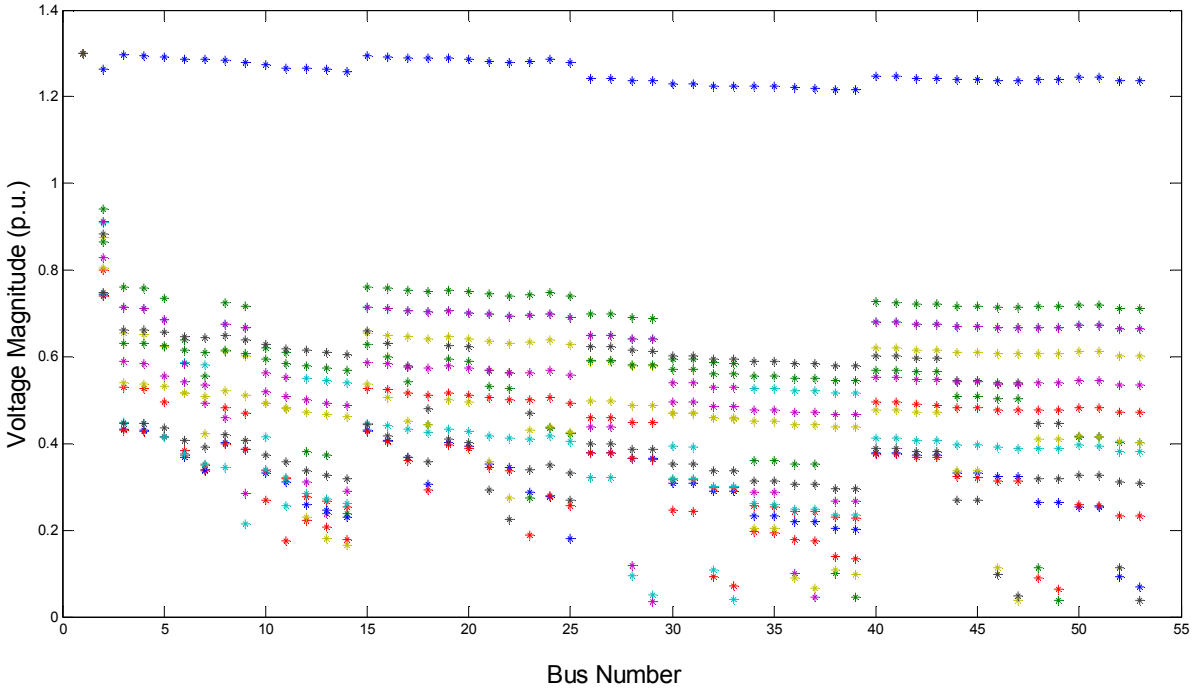

Figure 10. Voltage Magnitudes of 14 Solutions when V_{slack} =1.3 (p.u.)

Note that the same sequence of voltages at all the 53 buses is in the same color. The result shows only one solution would be considered as normal operating point since the voltage at all buses remain close to the slack bus voltage, which is the one on the top of Figure 10 in blue. The remaining 13 solutions are all mathematical solutions to the system

solved from the nonlinear power flow equations. But their voltage magnitudes are far below the slack bus voltage, an obvious huge gap between these solutions and the normal condition one is shown in Figure 10. At least one motor is under stall condition in these 13 solutions. One can not expect the distribution system to operate at these solutions. From the reasonable solution of the normal operating point, now the continuation method is applied again but with slack bus voltage magnitude as tracing parameter this time. An uncontrolled simulation is performed first, i.e., during the simulation process, the stalled induction motors are not switched to stall condition model. This is not strictly accurate since the motor slip is not allowed a value beyond one. But the results can indicate us whether any of the motors in the network would stall when the system voltage drops to a certain value, and this information is used in our following controlled simulation.

In Figure 11, each subplot shows the aggregate equivalent motor slip vs. slack bus voltage of all the traces during this simulation. Each of them has 14 cross points where slack bus voltage magnitude equals to 1.3 p.u., representing the different 14 solutions. We zoom in to look at loads, at bus 31 and bus 41 and results are as shown in Figure 12 and Figure 13 separately. For the motor at bus 31, it is clear to see that the motor slip remains low during the simulation. The value of the slip is between 0 and 0.03, which is within the normal operating range. However, for the motor at bus 41, although the slip remains low in the curves associated with 12 solutions, as shown at the bottom part of the plot, it shows stall characteristics during the tracing curve that links the two solutions, in the upper part of the plot. It shows that the slip starts around 0.7 and decreases a little bit while the slack bus

voltage decreasing, then after the turning point, it starts taking off and goes beyond one. Note that slip value of 0.7 is not a normal operating point for a motor.

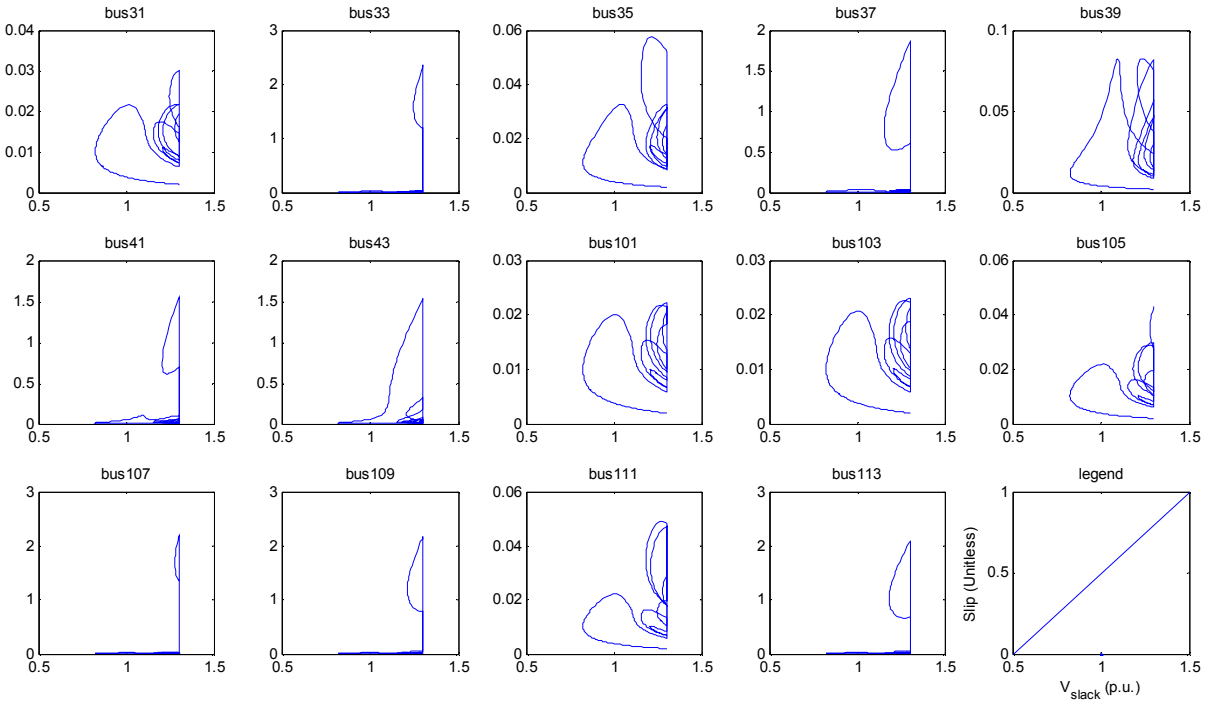

Figure 11. Slip – Voltage Curves of Motor Loads at All Buses in Uncontrolled Simulation

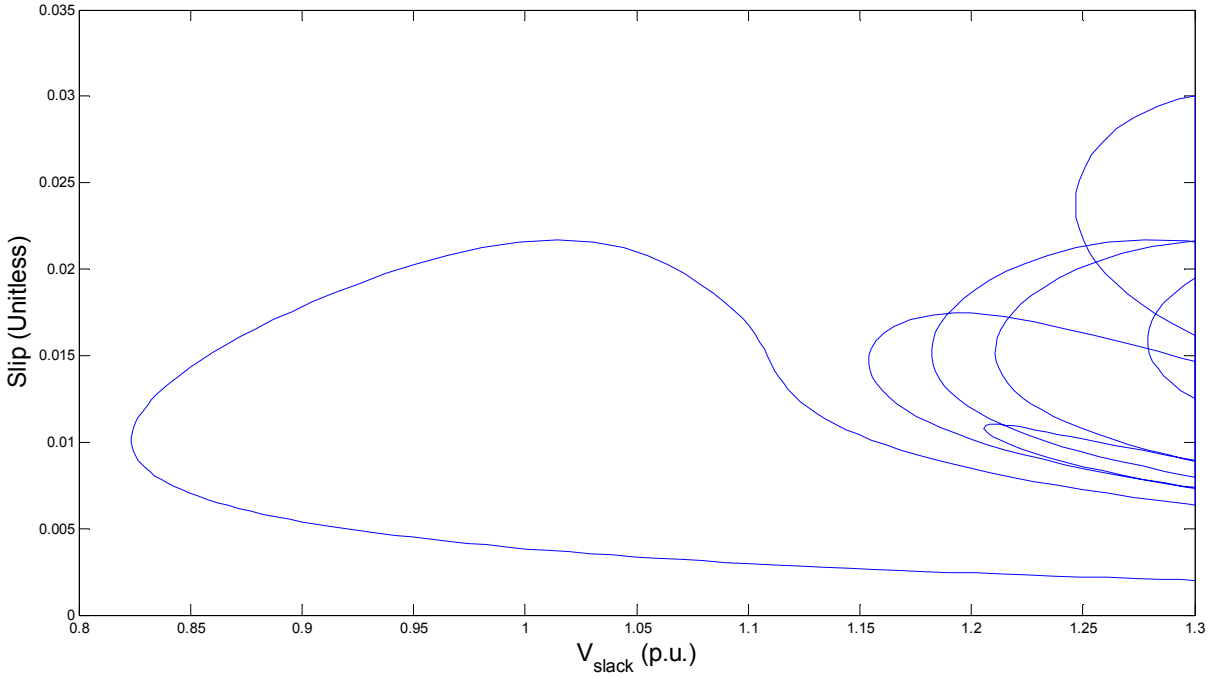

Figure 12. Slip – Voltage Curve of Motor Load at Bus 31 in Uncontrolled Simulation

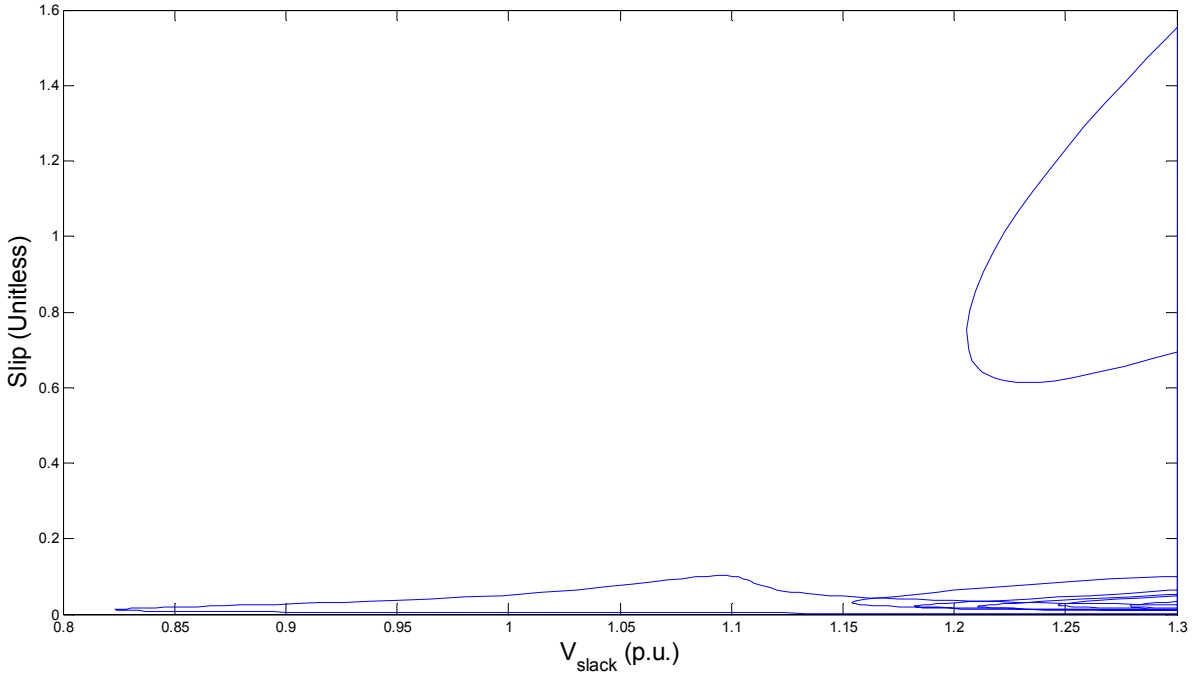

Figure 13. Slip – Voltage Curve of Motor Load at Bus 41 in Uncontrolled Simulation

Next a modified simulation is conducted, i.e., the stalled induction motors are switched to stall condition model during this process of decreasing slack bus voltage. After a certain motor stalls, it is set to stand still, equating the slip equals to one. This simulation is performed in sequence and eventually we get the results shown in the following figures.

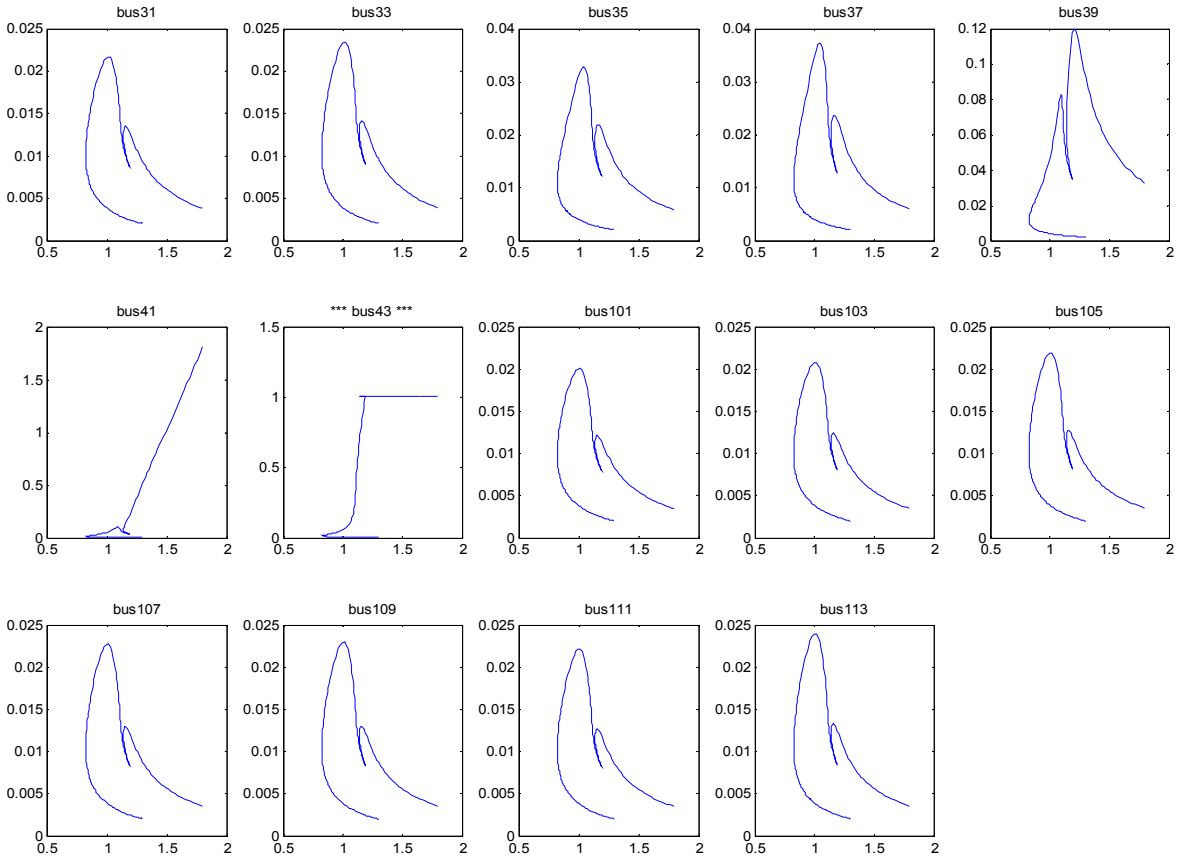

Figure 14. Slip – Voltage Curves of Motor Loads at All Buses in Controlled Simulation with One Motor Switched to Stall Condition Model (Bus 43)

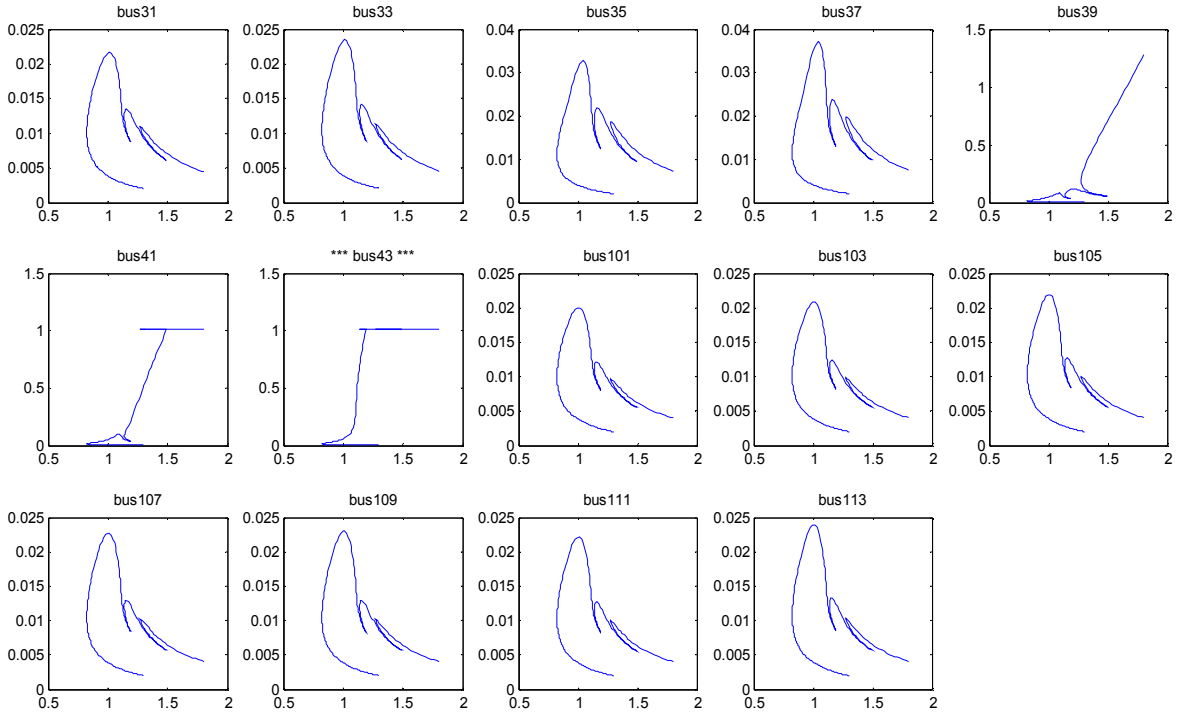

Figure 15. Slip – Voltage Curves of Motor Loads at All Buses in Controlled Simulation with Two Motors Switched to Stall Condition Model

Figure 14 shows the first stalled motor is at bus 43, which is the very last end bus of the upper first feeder of the distribution system. This makes sense because bus 43 probably has the weakest connection to the system voltage, and thus it would be the most "prone to stall" one. After the motor at bus 43 stalls, the slip of the motor is set to be one. Then we force the tracing direction of the continuation method to again decrease the slack bus voltage. As shown in the subplot for bus 41, the motor there remains stable for a little while, then it starts losing its stability and slowing down, eventually it will stall. The motor at bus 41 is the closest one to the stalled motor at bus 43 in the same feeder, which is also at an end bus.

In the following continuation routine, the motor at bus 41 is set to stall condition and tracing the curve with decreasing slack bus voltage again. Similarly, the result indicates that

motor at bus 39 is the next one that stalls, as shown in Figure 15. The same argument could be made for this result as for Figure 14. It is worth pointing out that the remaining motors which do not end up stalling during these routines experience back and forth in their values of slip.

We conduct the same procedure one after one, and the results show that the stalling of a number of induction motors does exacerbate the stalling of additional ones as discussed above. Furthermore, when the system reaches the point where five motors in the upper feeder are switched to stall condition, the next motor that stalls jumps to the other feeder instead of the motor close to the previous stalled ones in the same feeder. As shown in Figure 16, the motor at bus 113 would stall next, which is the one at the very last end of the lower feeder.

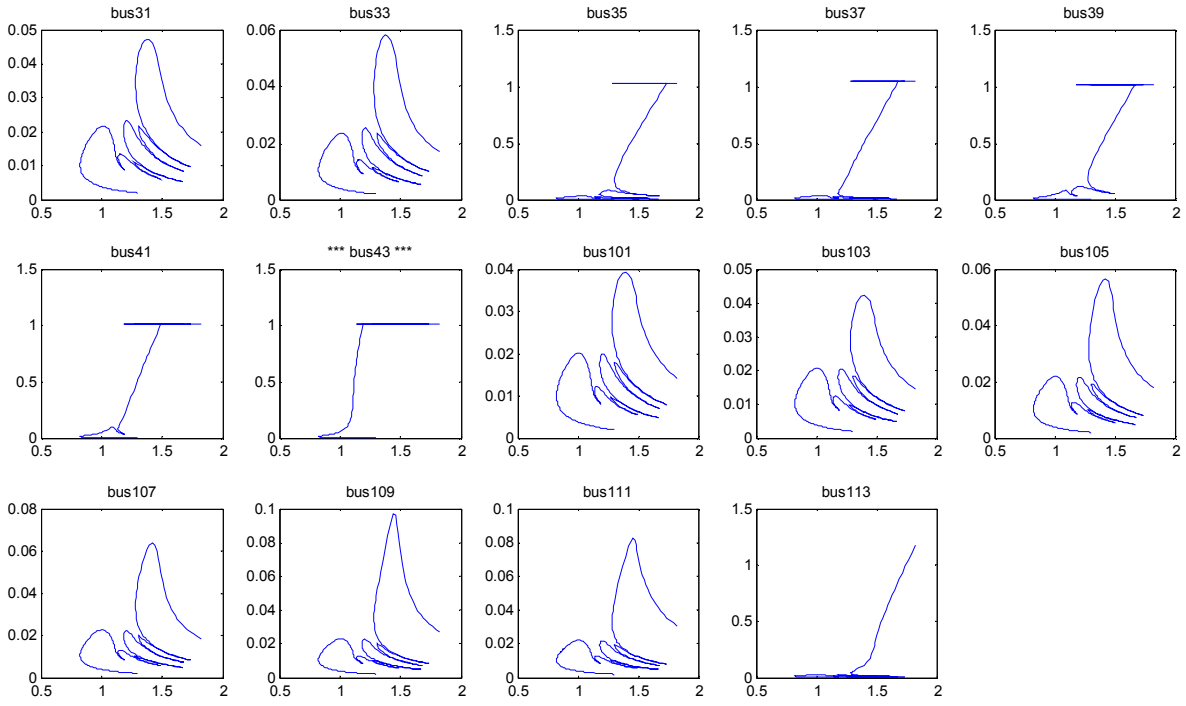

Figure 16. Slip – Voltage Curves of Motor Loads at All Buses in Controlled Simulation with Five Motors Switched to Stall Condition Model

Again, the motor at bus 113 is set to stall condition and tracing the curve with decreasing slack bus voltage in the following continuation routine. Based on our findings in the upper feeder, we expect motor at bus 111 to be the next one to stall since it is the one closest to the previous stalled on at bus 113. But very interestingly, the result indicates motor at bus 109 is the next one that stalls, as shown in Figure 17. When we look at the impedance of the distribution line linked bus 109 and bus 111 to the system, the later one has a smaller value, meaning bus 111 is stronger linked to the system than bus 109. Thus, it explains why the result happens to be this way.

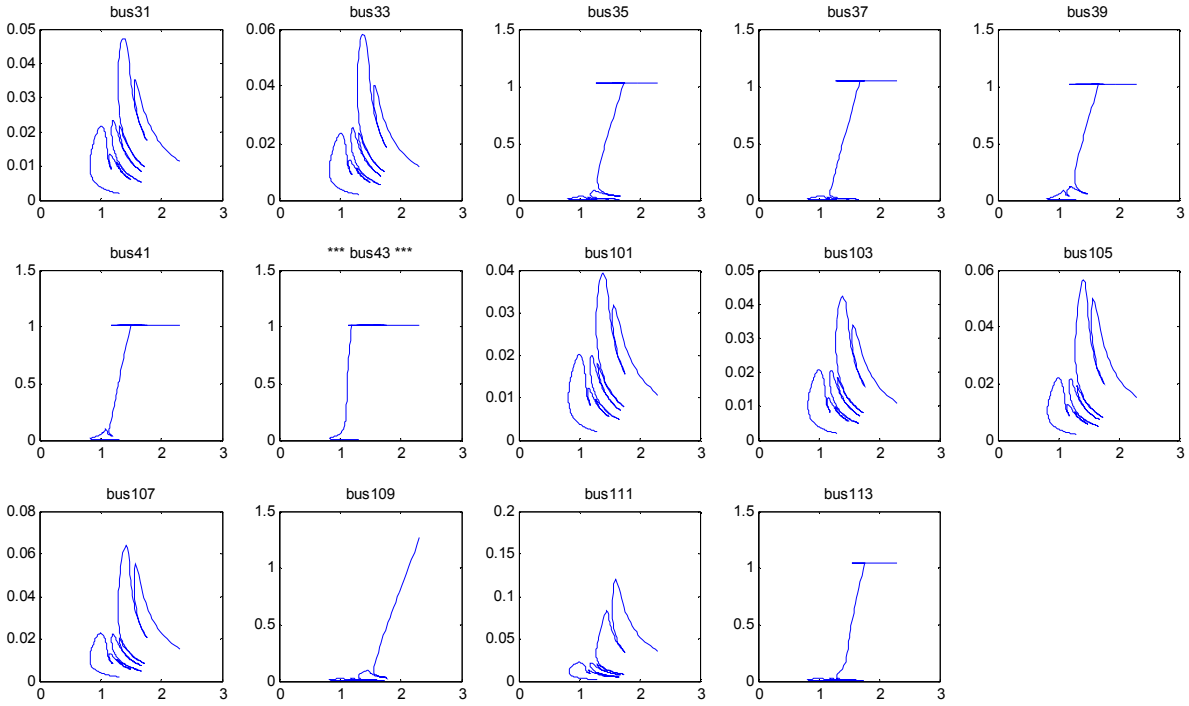

Figure 17. Slip – Voltage Curves of Motor Loads at All Buses in Controlled Simulation with Six Motors Switched to Stall Condition Model

Figure 18 shows that the stalling sequence of induction motors jumps back to the upper feeder after motor at bus 105 stalls. Again, this is due to how strong the motors are linked to the network.

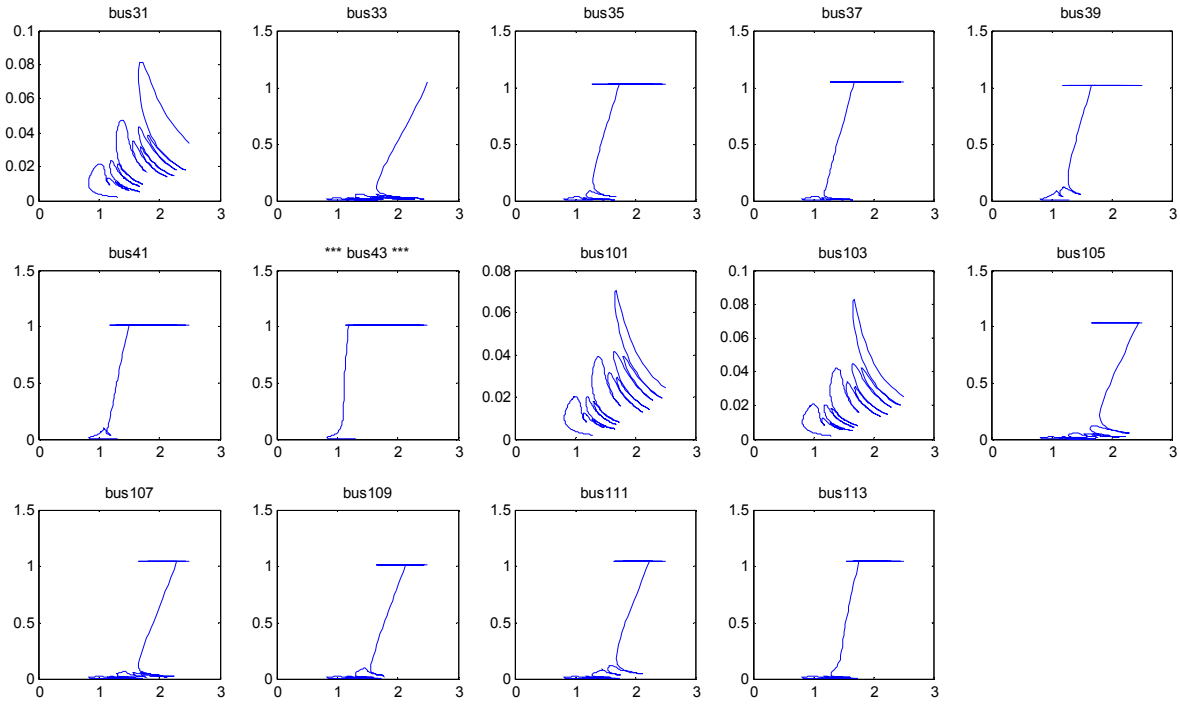

Figure 18. Slip – Voltage Curves of Motor Loads at All Buses in Controlled Simulation with Ten Motors Switched to Stall Condition Model

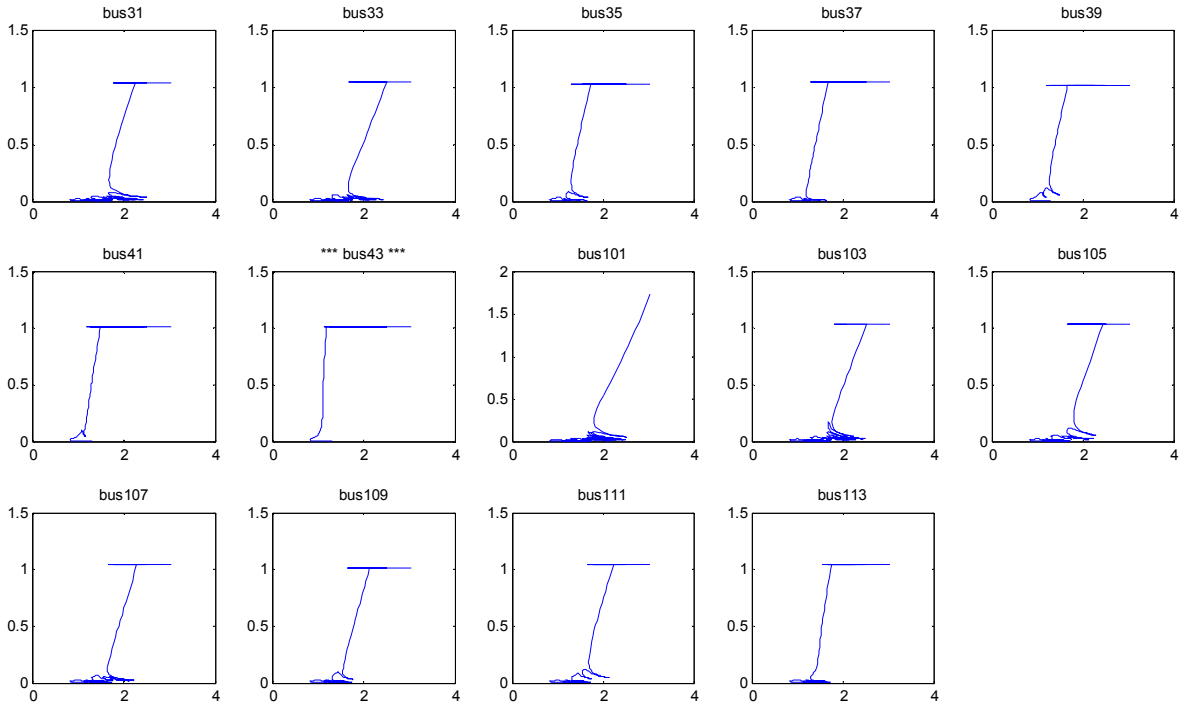

Figure 19. Slip – Voltage Curves of Motor Loads at All Buses in Controlled Simulation with Thirteen Motors Switched to Stall Condition Model

Eventually, all the motors in the distribution system would stall in sequential order, as shown in Figure 19. Furthermore, the associated motor terminal bus voltage magnitudes where the motors stall is in the range between 0.5 p.u. and 0.6 p.u., which matches the findings in [2].

With these curves calculated we examine the feasible solutions at 1.0 p.u. system voltage. We note that the only two stable solutions are with all motors operating normally, and all motors stalled. Thus we conclude for 100% motor load model, if a small number of motors tend to stall, all the motors will stall.

This scenario corresponds to an extreme motor load case. Next, we repeat this analysis with 50% motor load and 50% impedance load.

3.5 Scenario 2: Distribution Network with Fifty Percent Motor Loads

In this section, we analyze the 50% motor load and 50% impedance load model.

3.5.1 Distribution System Base Case Simulation with Fifty Percent Aggregate Induction Motor Loads and Reactive Power Compensation

Similar to section 3.4.1, a power flow case which matches the prefault system conditions is needed first. A constant impedance load is used to represent the other fifty percent of load. From the known base case, we can easily compute the value of Z_{load} from the bus voltage and power injection.

Like the previous scenario, additional reactive power compensation is for the induction motor model. The model with shunt capacitor bank is shown in Figure 20.

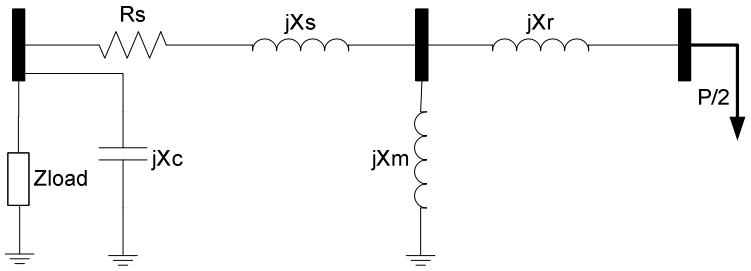

Figure 20. Modified Load Model with Fifty Percent Induction Motor Load and Reactive Power Compensation

With the reactive power compensation, steady-state power flow analysis is conducted, and the results are shown in Table 4. The solution is to the original condition, and this modified system is used for further analysis.

Table 4. Simulation Results of Distribution System Base Case with Fifty Percent Aggregate Induction Motor Loads after Reactive Power Compensation

Bus	Voltage		Generation		Load	
#	Mag(pu)	Ang(deg)	P (MW)	Q (MVAr)	P (MW)	Q (MVAr)
1	1.020	0.000	13.60	3.67	-	-
2	0.959	-7.451	-	-	-	-
3	0.967	-13.818	-	-	-	-
10	0.967	-13.821	-	-	-	-
11	0.963	-14.198	-	-	-	-
12	0.957	-15.316	-	-	-	-
13	0.955	-16.011	-	-	-	-
21	0.956	-14.328	-	-	-	-
22	0.949	-14.494	-	-	-	-
23	0.943	-15.657	-	-	-	-
24	0.937	-15.844	-	-	-	-
25	0.934	-16.400	-	-	-	-
26	0.930	-16.442	-	-	-	-
27	0.927	-16.558	-	-	-	-
80	0.967	-13.817	-	-	-	-
81	0.963	-14.173	-	-	-	-
82	0.959	-14.702	-	-	-	-
83	0.957	-15.400	-	-	-	-
91	0.959	-14.218	-	-	-	-
92	0.956	-14.262	-	-	-	-
93	0.952	-14.783	-	-	-	-
94	0.948	-14.825	-	-	-	-
95	0.951	-15.557	-	-	-	-
96	0.954	-15.459	-	-	-	-
97	0.947	-15.614	-	-	-	-
30	0.925	-13.263	-	-	-	-
31	0.925	-13.397	-	-	0.50	0.00
32	0.918	-13.431	-	-	-	-
33	0.918	-13.568	-	-	0.50	0.00
34	0.912	-14.597	-	-	-	-
35	0.912	-14.735	-	-	0.50	0.00
36	0.906	-14.787	-	-	-	-
37	0.906	-14.927	-	-	0.50	0.00

38	0.903	-15.344	-	-	-	-
39	0.903	-15.484	-	-	0.50	0.00
40	0.900	-15.387	-	-	-	-
41	0.900	-15.528	-	-	0.50	0.00
42	0.897	-15.504	-	-	-	-
43	0.897	-15.647	-	-	0.50	0.00
100	0.928	-13.152	-	-	-	-
101	0.928	-13.286	-	-	0.50	0.00
102	0.924	-13.198	-	-	-	-
103	0.924	-13.332	-	-	0.50	0.00
104	0.921	-13.720	-	-	-	-
105	0.920	-13.855	-	-	0.50	0.00
106	0.917	-13.763	-	-	-	-
107	0.917	-13.900	-	-	0.50	0.00
108	0.919	-14.495	-	-	-	-
109	0.919	-14.631	-	-	0.50	0.00
110	0.923	-14.395	-	-	-	-
111	0.923	-14.530	-	-	0.50	0.00
112	0.916	-14.553	-	-	-	-
113	0.916	-14.690	-	-	0.50	0.00
			--------	--------	--------	--------
		Total:	13.60	3.67	7.00	0.00

3.5.2 Simulation and Results of Induction Motor Stalling in FIDVR

Finding all the solutions of the modified system in section 3.5.1 is our first interest. In this case, 26 solutions are found after 1282 tracing processes when slack bus voltage equal to 1 per unit. The voltage magnitudes of these 14 solutions are shown in Figure 21.

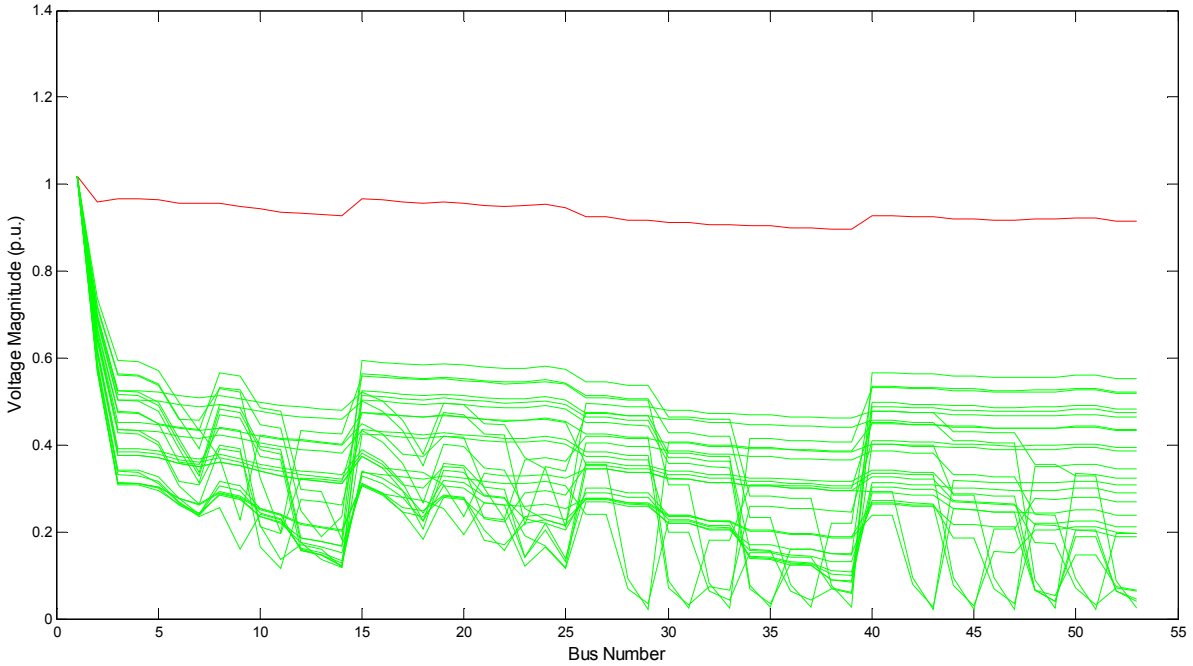

Figure 21. Voltage Magnitudes of 26 Solutions when V_{slack} =1 (p.u.)

Note that the same sequence of voltages at all the 53 buses is linked together in the same color. Only one solution (in red) is a physical normal operating point. The remaining 25 solutions are all mathematical solutions to the system solved from the nonlinear power flow equations. Analysis shows that at least one motor is under stall condition in these 25 solutions.

Next the continuation method is applied with slack bus voltage magnitude as tracing parameter this time. The stalled induction motors are switched to stall condition model during this process of decreasing slack bus voltage. As before, each subplot in the resulting figures shows the aggregate equivalent motor slip vs. slack bus voltage during this simulation.

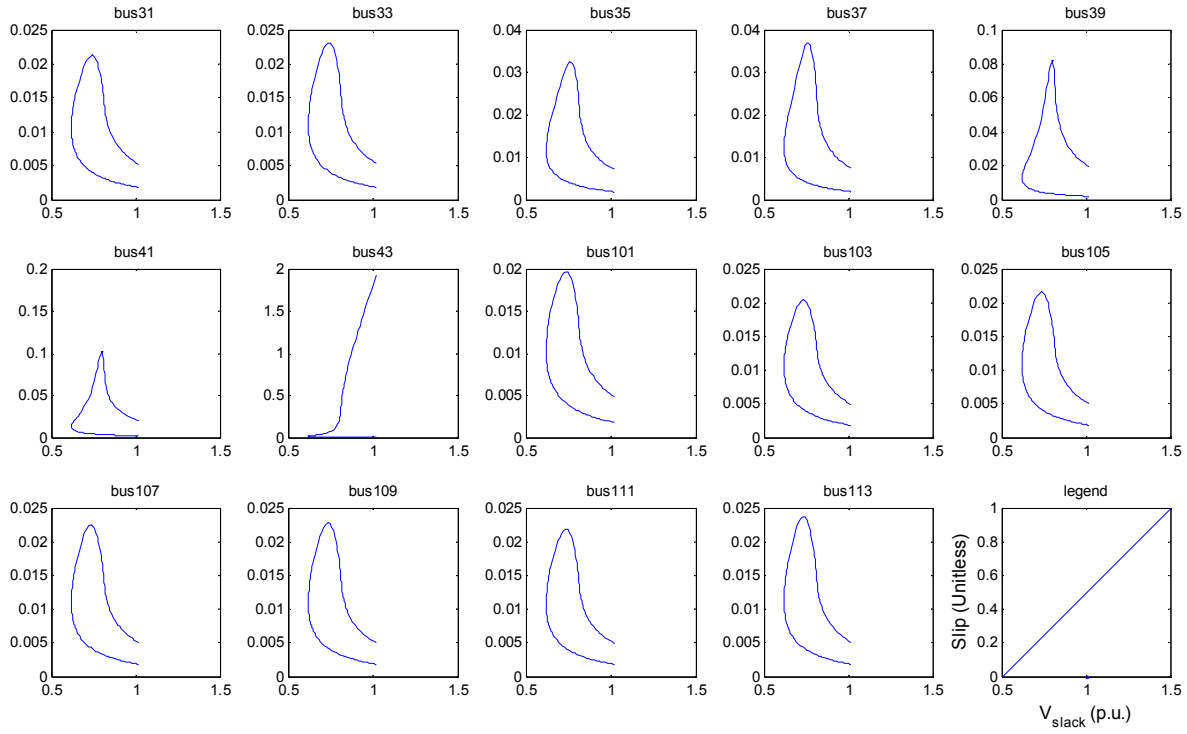

Figure 22. Slip – Voltage Curves of Motor Loads at All Buses in Controlled Simulation

Figure 23 shows the first stalled motor is at bus 43, matching the result of the 100% motor load scenario. When the slack bus voltage equals to one, the other motors stay stable, so there is a stable solution where the system can operate normally with the stalling of the motor at bus 43.

After the motor at bus 43 stalls, its slip is set to be one. Then we force the tracing direction of the continuation method to decrease the slack bus voltage again. The results are given in Figure 23. The motor at bus 41 is the next one to stall, but still, others remain stable at normal voltage.

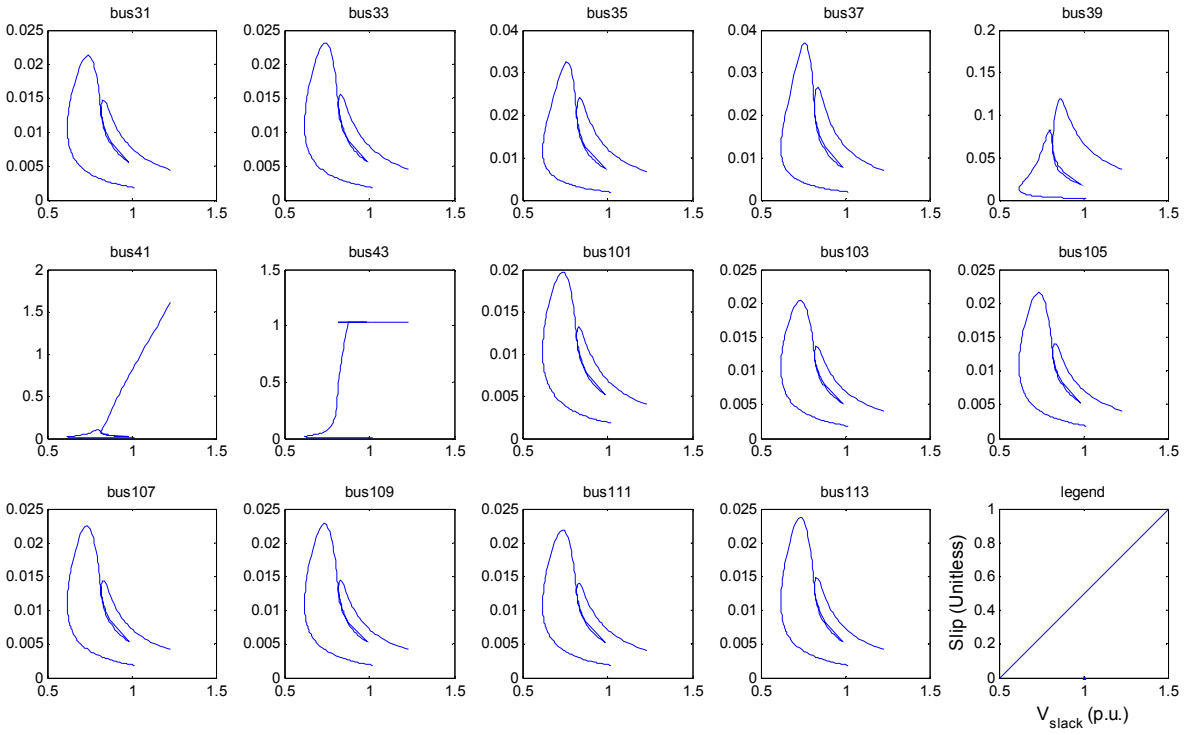

Figure 23. Slip – Voltage Curves of Motor Loads at All Buses in Controlled Simulation with One Motor Switched to Stall Condition Model

Eventually, when there are five motors are stalling in the first feeder, as shown in Figure 24, the system can still have a physical operating point around 1 per unit with the five stalled motors.

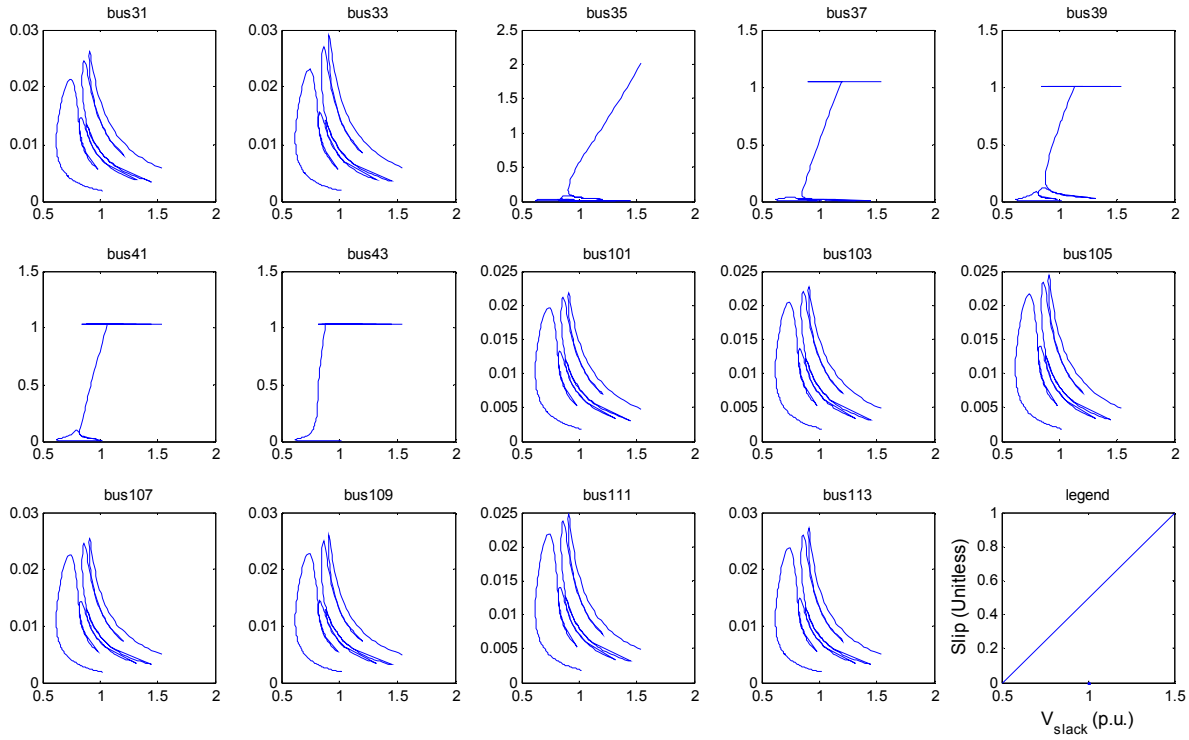

Figure 24. Slip – Voltage Curves of Motor Loads at All Buses in Controlled Simulation with Four Motors Switched to Stall Condition Model

However, the following stalled motor jumps to the other feeder, at bus 113. This additional stalled motor actually results in losing the stable operating point of the distribution system. As shown in Figure 25, the other motors are in their unstable operating range when slack bus equals to one, given six stalled motors. Thus, for this distribution system with fifty percent induction motor loads, the maximum stalled motor it can take is five, and the system will lose stability with one additional stalled motor.

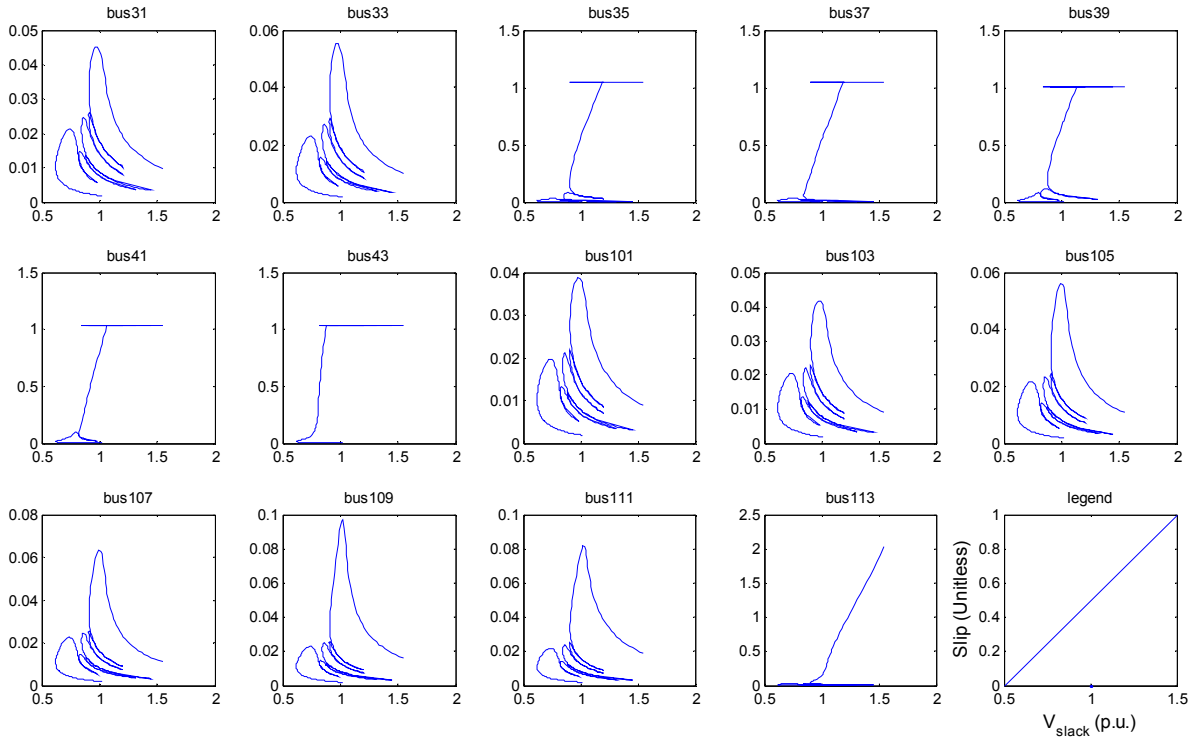

Figure 25. Slip – Voltage Curves of Motor Loads at All Buses in Controlled Simulation with Five Motors Switched to Stall Condition Model

Figure 26 shows that the stalling sequence of induction motors jumps back to the upper feeder after motor at bus 105 stalls. Similar to scenario one, this is basically due to how strong the motors are linked to the network.

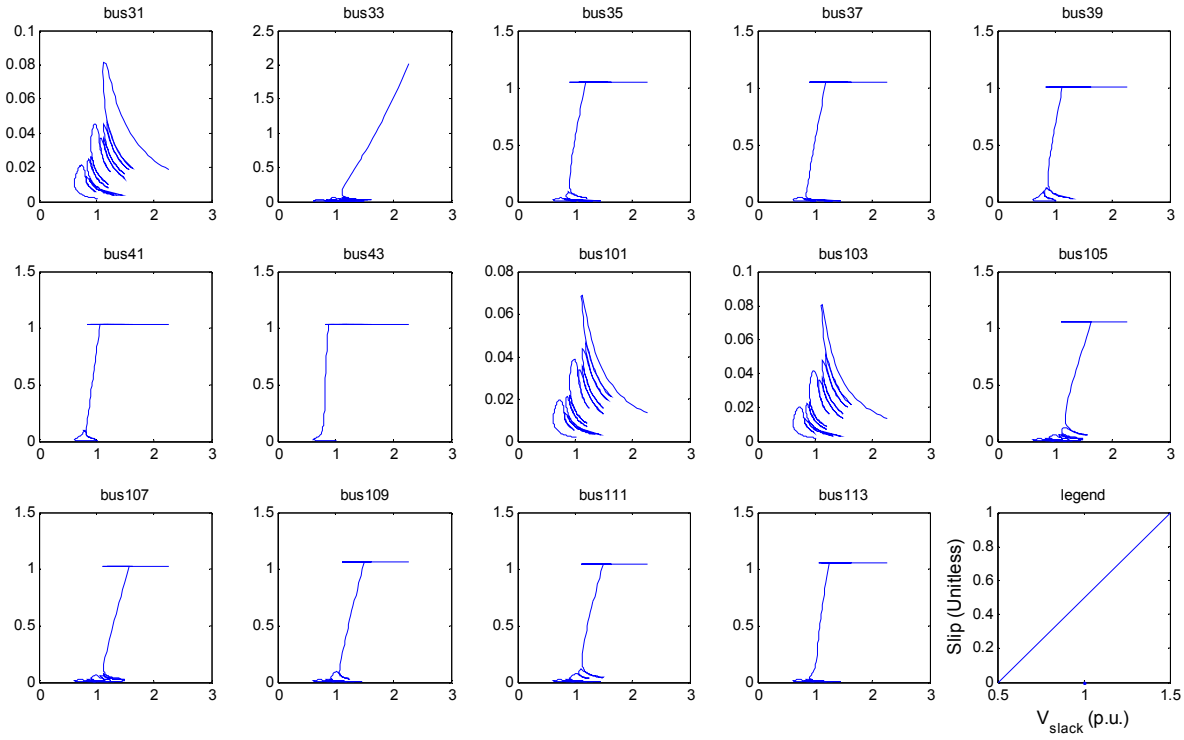

Figure 26. Slip – Voltage Curves of Motor Loads at All Buses in Controlled Simulation with Ten Motors Switched to Stall Condition Model

Eventually, all the motors in the distribution system are set to stall condition in a cascaded matter, as shown in Figure 27.

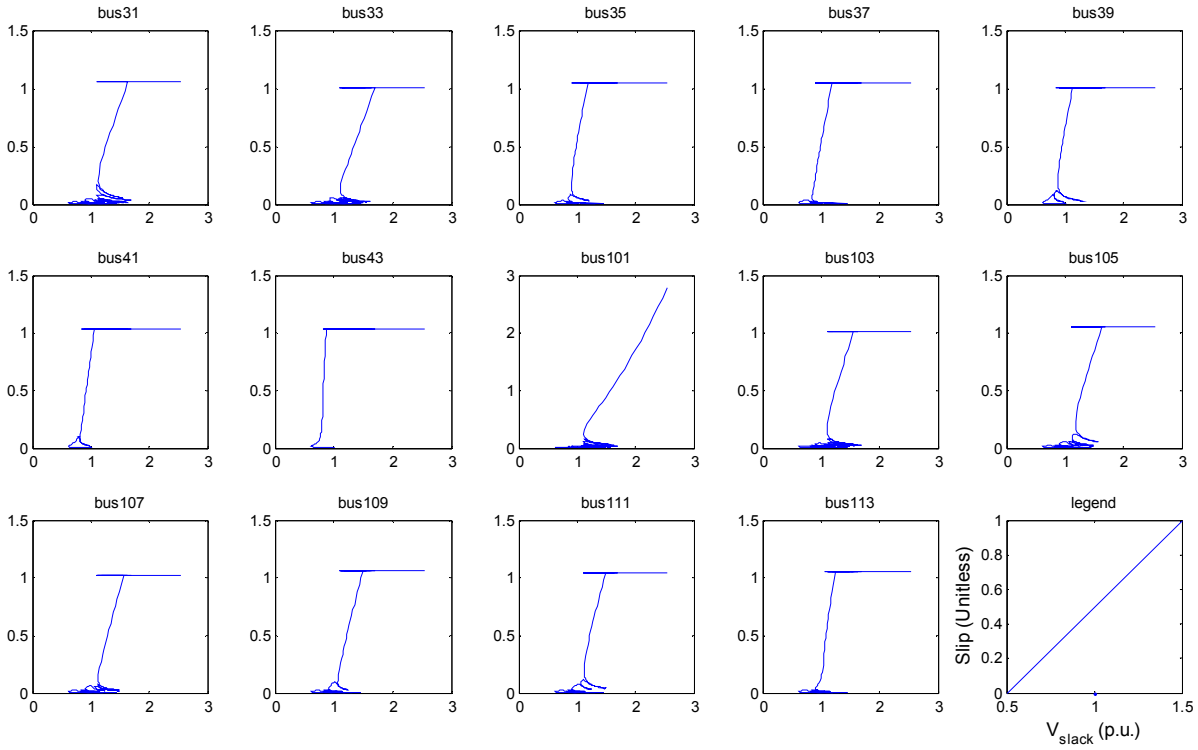

Figure 27. Slip – Voltage Curves of Motor Loads at All Buses in Controlled Simulation with Thirteen Motors Switched to Stall Condition Model

The 50% motor/50% impedance load shows the possibility of some motor stall without complete motor stall, at normal system voltage. A maximum 5 motor stall is allowed, beyond which, the only stable solution is all motor stalled.

Since there are 14 loads total, this system may allow up to approximately 36% motor stalled. While this may sound optimistic, if all motors are similarly likely to stall, approximately 64% of these "prone to stall" motors would need to be replaced by more "robust to stall" motors.

A more detailed model would examine the best locations along the feeder to place robust motors to mitigate complete stall.

4. Conclusion

This thesis studies the possibility that the stalling of a small percentage of induction motors could precipitate FIDVR events. A 12.5kV distribution network model with A/C motor load is used to construct certain bifurcation diagrams. Two approaches are performed. Firstly, the algorithm based on the analysis of the topological structures of the solution set defined by the parameterized load flow equations is implemented to find all the solutions to load flow equations at a particular voltage level. Continuation power flow based on predictor-corrector technique, is conducted as the second approach to arrive at system steady-state solutions tracing the curves of motor behavior while the system bus voltage is varied.

The stable and unstable operating points of induction machines are obtained and analyzed. Results show that a small percentage of induction motors stalling could exacerbate the stalling of additional motors. For scenario 1, with one hundred percent motor loads, there are no stable solutions for the system with a partial number of A/C motors stalled. For scenario 2, with fifty percent motor load and fifty percent constant impedance load, the system has a stable operating point with up to five stalled motors, out of a total of fourteen.

Based on our work, we conclude that a small percentage of stalled induction motors in practice could precipitate the stalling of additional motors, or even all motors in a distribution network. Thus, a mitigation strategy of replacing a number of "prone to stall" motors to "robust" ones may not effective. This information is crucial in developing mitigation plans to avoid a FIDVR event.

Future work could involve using the continuation method to determine a threshold of the percentage of induction motor loads integrated into a system where it will lose stability.

Development of a more accurate aggregate motor model, and a composite load model suitable for system wide dynamic simulation studies is another aspect to look at. The model may be eventually used for either detailed planning studies or for validation studies of other approaches to dynamic load modeling.

Also, a more detailed study could investigate the advantage of placement of robust motor to replace prone to stall motors. Some locations may be better than others. Intuitively one would expect that stalled motor near the beginning of the feeder are worse than at the end.

5. Appendix

The author in [1] claims that any solution of the load flow is reachable from all other solutions via the manifolds. In the proof for Theorem 2 in section 2.4 of [1], the author states the following:

The load flow equations $f(x) = 0$ *contains:*

$$f_m(\delta_m, \delta, V) - P_m = 0 \tag{1}$$

$$f_p(\delta_m, \delta, V) - P = 0 \tag{2}$$

$$f_q(\delta_m, \delta, V) - Q = 0 \tag{3}$$

Just consider the active power balance equation on load buses, we have

$$v_i^2 G_{ii} + v_i \sum_{j \in I_m} E_j y_{ij} \cos\left(\delta_i - \delta_{mj} - \theta_{ij}\right)$$

$$+ v_i \sum_{j \in I_l, j \neq i} v_j y_{ij} \cos\left(\delta_i - \delta_j - \theta_{ij}\right) - p_i = 0$$

$$i = 1, \dots, n_l \tag{4}$$

In terms of the voltage v*, these equations are a system of quadratic polynomials, so the voltage* v_i *can be written as follows:*

$$v_i = \frac{-\sigma_{ci}(x_i) \pm \sqrt{\sigma_{ci}(x_i)^2 - 4G_{ii}p_i}}{2G_{ii}} \tag{5}$$

where

$$\sigma_{ci} = \sum_{j \in I_m} E_j y_{ij} \cos(\delta_i - \delta_{mj} - \theta_{ij}) + v_i \sum_{j \in I_l, j \neq i} v_j y_{ij} \cos(\delta_i - \delta_j - \theta_{ij}) \quad (6)$$

Similarly, active power balance on a generator bus is represented by the following equation:

$$E_i^2 G_{ii} + E_i \sum_{j \in I_l} v_j y_{ij} \cos(\delta_{mi} - \delta_j - \theta_{ij}) - p_i = 0$$

$$i = 1, \ldots, n_g \quad (7)$$

The voltage E_i can be written as follows:

$$E_i = \frac{-\sigma_{ci}(x_i) \pm \sqrt{\sigma_{ci}(x_i)^2 + 4G_{ii}p_i}}{2G_{ii}} \quad (8)$$

where

$$\sigma_{ci} = \sum_{j \in I_l} v_j y_{ij} \cos(\delta_{mi} - \delta_j - \theta_{ij}) \quad (9)$$

Only one of the plus and minus signs is applicable for a particular load flow solution. We link each load flow solution x with a binary number in the following way. For the voltage vector v in x, if v_i is written in (5) with a plus sign in front of the square root, we assign a binary digit "0" to this v_i; if vi has a minus sign in front of the square root, we assign a binary digit "1" to v_i. Since the vector v has n_l components, the binary number is n_l bits long.

The author states that "It is obvious that each solutions can be uniquely identified by the binary labels." We argue that this claim is wrong. A counter example is given below. The completeness proof relies on this uniqueness property. Since, by the counter example below, we show that the asserted property is false, the method has not been proven to find all solutions. Nevertheless, the method may find all the solutions, even if not proven to do so. We have found no counter examples to the method.

Figure 28 shows a simple three bus test system, the line parameters and loads are specified as shown in per unit.

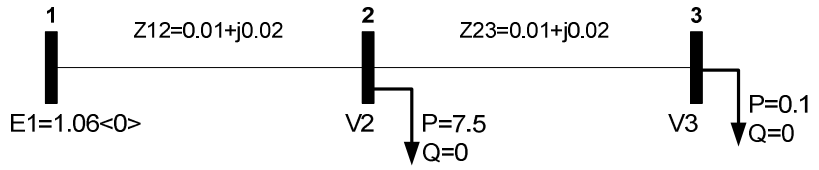

Figure 28. 3 Bus Test System

After applying the author's technique of finding all the solutions, four solutions are found, as listed in Table 5 below.

Table 5. Solutions for the 3 Bus Test System

Solution Number	E1 (p.u.<degree>)	V2 (p.u. <degree>)	V3 (p.u. <degree>)
Solution 1	1.06 <0>	0.9700 <-8.5013>	0.9690 <-8.6232>
Solution 2	1.06 <0>	0.1753 <-54.8780>	0.1690 <-58.7476>
Solution 3	1.06 <0>	0.2090 <-43.3045>	0.0110 <-104.0492>
Solution 4	1.06 <0>	0.4039 <-20.7915>	0.0056 <-83.5197>

Then we plug in these solutions accordingly, and calculate the square root terms in equation (5) and the values for v_i, the results are shown in below with the solutions bolded.

Table 6. Calculated Values for E_i and v_i in Equation (5) and (8) Using Active Power Balance

	Plus sign "0"			Minus sign "1"		
Solution #	|E1| (p.u.)	|V2| (p.u.)	|V3| (p.u.)	|E1| (p.u.)	|V2| (p.u.)	|V3| (p.u.)
Solution 1	**1.0599**	**0.9700**	**0.9690**	-0.3873	0.1933	0.0052
Solution 2	**1.0599**	1.0695	**0.1690**	-1.2458	**0.1753**	0.0296
Solution 3	**1.0601**	0.8967	0.4559	-1.1947	**0.2091**	**0.0110**
Solution 4	**1.0601**	0.4637	0.8975	-0.9692	**0.4043**	**0.0056**

Similarly, if we redo this using reactive power balance equations, we have:

Table 7. Calculated Values for E_i and v_i in Equation (5) and (8) Using Reactive Power Balance

	Plus sign "0"			Minus sign "1"		
Solution #	|E1| (p.u.)	|V2| (p.u.)	|V3| (p.u.)	|E1| (p.u.)	|V2| (p.u.)	|V3| (p.u.)
Solution 1	**1.0600**	**0.9700**	**0.9690**	-0.0290	0	0
Solution 2	**1.0600**	**0.1753**	**0.1690**	-0.8875	0	0
Solution 3	**1.0599**	**0.2090**	**0.0110**	-0.8362	0	0
Solution 4	**1.0599**	**0.4039**	**0.0056**	-0.6107	0	0

By matching the values in Table 5 and Table 6 with Table 4, we can get the binary combinations for the 4 solutions of the 3 bus test system as follows:

Table 8. Binary combinations for the 4 solutions

	Using Active Power Balance			**Using Reactive Power Balance**		
Solution #	|E1|	|V2|	|V3|	|E1|	|V2|	|V3|
Solution 1	0	0	0	0	0	0
Solution 2	0	1	0	0	0	0
Solution 3	0	1	1	0	0	0
Solution 4	0	1	1	0	0	0

The results in Table 8 clearly indicate that the same binary label could identify different solutions, which is a contradiction to the author's statement.

6. References

[1] Weimin Ma, “Dynamical systems analysis in electric power systems”, Ph.D. Dissertation, Cornell University, Ithaca, NY, August, 1991.

[2] B.R. Williams, W.R. Schmus and D.C. Dawson, “Transmission voltage recovery delayed by stalled air conditioner compressors, *Power Systems, IEEE Transactions on*, vol. 7, no. 3, pp. 1173-1181, August 1992.

[3] NERC Technical Reference Paper – Fault-Induced Delayed Voltage Recovery (FIDVR), June 2009.

[4] J.W. Shaffer, “Air conditioner response to transmission faults,” *Power Systems, IEEE Transactions on*, vol. 12, no. 2, pp. 614-621, May 1997.

[5] U.S. Department of Energy – Industry Workshop on The Role of Residential AC in Contributing to Fault-Induced Delayed Voltage Recovery, Dallas, Texas, April 2008.

[6] General Electric Company, "Load Modeling for Power Flow and Transient Stability Computer Studies," Vol. 1 - 4, EPRl Report EL-5003, 1987, Vol. 1 page 3-26.

[7] W.W. Price, F. Nozari, A. Murdoch, et al., Summary Report on the EPRI Project RP849-7.

[8] F. Nozari, M. D. Kankam and W. W. Price, "Aggregation of Induction Motors for Transient Stability Load Modeling," *Power Systems, IEEE Transactions on*, vol. 2, pp. 1096-1103, 1987.

[9] R. D. Zimmerman, C. E. Murillo-Sanchez, and R. J. Thomas, “MATPOWER's Extensible Optimal Power Flow Architecture," *in Power and Energy Society General Meeting, 2009 IEEE*, pp. 1-7, July 26-30 2009.

[10] IEEE WG on Voltage Stability, *Suggested techniques for voltage stability analysis*. Piscataway, NJ: 1993.

[11] W. Ma and J. S. Thorp, "An efficient algorithm to locate all the load flow solutions," *Power Systems, IEEE Transactions on*, vol. 8, pp. 1077-1083, 1993.

[12] C. A. Canizares and F. L. Alvarado, "Point of collapse and continuation methods for large AC/DC systems," *Power Systems, IEEE Transactions on*, vol. 8, pp. 1-8, 1993.

[13] K. Iba, H. Suzuki, M. Egawa and T. Watanabe, "Calculation of critical loading condition with nose curve using homotopy continuation method," *Power Systems, IEEE Transactions on*, vol. 6, pp. 584-593, 1991.

[14] Y. Tamura, H. Mori and S. Iwamoto, "Relationship Between Voltage Instability and Multiple Load FLow Solutions in Electric Power Systems," *Power Apparatus and Systems,* IEEE Transactions on, vol. PAS-102, pp. 1115-1125, 1983.

[15] V. Ajjarapu and C. Christy, "The continuation power flow: A tool for steady state voltage stability analysis," *in Power Industry Computer Application Conference, 1991. Conference Proceedings*, 1991, pp. 304-311.

[16] B. Lesieutre, D. Kosterev and J. Undrill, “Phasor modeling approach for single phase A/C motors,” *in Proceedings of the IEEE PES General Meeting*, July 2008.

[17] R. Seydel: World of Bifurcation. Online Collection and Tutorials of Nonlinear Phenomena. WOB99, 1999. Available: http://www.bifurcation.de/tutorials.html